OLD DOMINION UNIVERSITY RESEARCH FOUNDATION

DEPARTMENT OF MECHANICAL ENGINEERING AND MECHANICS
SCHOOL OF ENGINEERING
OLD DOMINION UNIVERSITY
NORFOLK, VIRGINIA

FEASIBILITY OF QUASI-RANDOM BAND MODEL IN EVALUATING ATMOSPHERIC RADIANCE

By

S.N. Tiwari, Principal Investigator

and

Navin Mirakhur

Final Report
For the period ending June 30, 1980

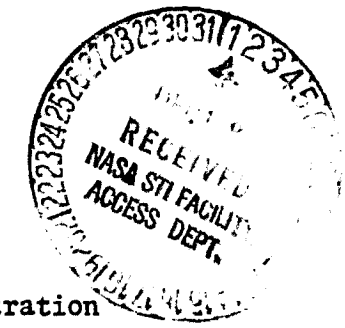

Prepared for the
National Aeronautics and Space Administration
Langley Research Center
Hampton, Virginia

Under
Research Grant NSG-1522
John T. Suttles, Technical Monitor
Atmospheric Environmental Sciences Division

August 1980

DEPARTMENT OF MECHANICAL ENGINEERING AND MECHANICS
SCHOOL OF ENGINEERING
OLD DOMINION UNIVERSITY
NORFOLK, VIRGINIA

FEASIBILITY OF QUASI-RANDOM BAND MODEL IN EVALUATING ATMOSPHERIC RADIANCE

By

S.N. Tiwari, Principal Investigator

and

Navin Mirakhur

Final Report
For the period ending June 30, 1980

Prepared for the
National Aeronautics and Space Administration
Langley Research Center
Hampton, Virginia 23665

Under
Research Grant NSG-1522
John T. Suttles, Technical Monitor
Atmospheric Environmental Sciences Division

Submitted by the
Old Dominion University Research Foundation
P.O. Box 6369
Norfolk, Virginia 23508

August 1980

FOREWORD

This report covers the final work completed on the research project "Radiative Transfer Models for the Earth Radiation Budget and Climatic Studies." The work was supported by the NASA/Langley Research Center (Experiment Analysis Branch of the Atmospheric Environmental Sciences Division) through research grant NSG 1522. The grant was monitored by John T. Suttles of the Atmospheric Environmental Sciences Division.

TABLE OF CONTENTS

LIST OF TABLES

LIST OF FIGURES

LIST OF FIGURES - CONCLUDED

FEASIBILITY OF QUASI RANDOM-BAND MODEL IN EVALUATING ATMOSPHERIC RADIANCE

By

S.N. Tiwari[1] and Navin Mirakhur[2]

SUMMARY

The use of the quasi-random band model in evaluating upwelling atmospheric radiation is investigated. The spectral transmittance and total band absorptance are evaluated for selected molecular bands by using the line-by-line model, quasi-random band model, exponential sum fit method, and empirical correlations, and these are compared with the available experimental results. The atmospheric transmittance and upwelling radiance have been calculated by using the line-by-line and quasi-random band models and are compared with the results of an existing program called LOWTRAN. The results obtained by the exponential sum fit and empirical relations are not in good agreement with experimental results and their use cannot be justified for atmospheric studies. The line-by-line model is found to be the best model for atmospheric applications, but it is not practical because of high computational costs. The results of the quasi-random band model compare well with the line-by-line and experimental results. The use of the quasi-random band model is recommended for evaluation of the atmospheric radiation.

---

[1]Eminent Professor, Department of Mechanical Engineering and Mechanics, Old Dominion University, Norfolk, Virginia 23508.

[2]Graduate Research Assistant, Department of Mechanical Engineering and Mechanics, Old Dominion University, Norfolk, Virginia 23508.

INTRODUCTION

Extensive study of the radiative transfer phenomena in the Earth's atmospheric system has been carried out in the last two decades (refs. 1 to 4). This is important for the understanding of the meteorological process on all scales and the spatial variation in surface temperature in the Earth atmosphere. Techniques for measuring the Earth's surface temperature include airborne instruments and satellite-mounted radiometers. In order to understand and interpret the instrument performance and readings, it is desirable to develop radiation models and numerical techniques that account for the absorption and attenuation of actual atmospheric radiation. Development of accurate models for radiative transfer in the atmosphere is extremely important for the Earth radiation budget studies (refs. 4 to 6). These models have to be used for simulation and interpretation of Earth radiation budget measurements as well as for retrieval of various surface and the atmospheric parameters from satellite-measured radiances (ref. 7). Since the radiation budget of the planet has been identified as an important element of the climate system, its measurements are being attempted with increasing accuracy (refs. 8, 9). As a result, considerable improvement is warranted in the accuracy of the theoretical models dealing with atmospheric radiation transfer.

Many models for radiation absorption by molecular gases are available in the literature. The simplest one is the gray gas model (or the emissivity approximation) and the most sophisticated and accurate one is the line-by-line (LBL) model (or the direct integration procedure). Between the emissivity approximation and direct integration method lie several narrow and wide band models and band model correlations which vary greatly in complexity and accuracy. A comprehensive review on various line and band models is available in reference 4. Use of either an LBL model or a narrow band model is suggested for most atmospheric applications. The narrow band models usually recommended for atmospheric studies are the Elsasser (or regular) model, statistical (Meyer-Goody or Goody) model, and quasi-random band (QRB) model. The QRB is probably the best band model to represent accurately the absorption of a vibration-rotation band

and is suitable for calculating the atmospheric transmittance and upwelling radiance. The fundamental features of the QRB are discussed, in detail, in references 10 to 12, and the procedure for calculating the atmospheric transmittance and upwelling radiance is given in reference 12. In spectral ranges where both line absorption and scattering are important, a widely used approximation for calculating spectrally integrated radiative flux is the exponential-sum fitting of transmissions (ESFT) method. The basis for this method is that the transmission function for a given spectral interval is fit by a sum of exponentials. The method is described in reference 13.

Radiative transfer models used in earlier climatic investigations employed radiation charts, generalized absorption coefficients, and emissivity approximations (refs. 5, 14-16). Rodgers (ref. 17) has indicated that the use of multi-interval narrow-band radiative transfer schemes in climate modeling studies will constitute a significant step forward and result in improved accuracy of the model output. Fels and Kaplan (ref. 18) have investigated the effects of using different radiative transfer schemes on the thermal structure of the atmosphere and its consequences to atmospheric dynamics. They employed two different radiative absorption models, the emissivity approximation, and Goody's statistical band formulation, and performed numerical experiments with the NCAR general circulation model. They observed a significant difference in the cooling rates in the two experiments which resulted in significantly different mean temperature fields and meridional circulations.

Very high accuracy can be achieved in the radiation computation by using the LBL integration procedure in the radiative transfer models (ref. 19). However, the procedure is too cumbersome and makes excessive demands on computer time. Tiwari and Gupta (ref. 20) have shown that the QRB model can be used for computing atmospheric transmittances with accuracy comparable to that of the LBL method and with computer usage more than an order of magnitude smaller. Kunde (ref. 11) has also used this model to compute outgoing infrared radiances from planetary atmospheres. However, before use of the QRB model can be recommended for Earth radiation budget and climate modeling studies, further work needs to be done to validate the model on a sound basis. This model should be used for absorption bands of different species in different spectral ranges. It is quite possible

that the model is not justified at shorter wave lengths and smaller pressure path lengths. Furthermore, under realistic atmospheric conditions, the model may give good results in certain spectral ranges but is poor in other ranges.

The objective of this study is to validate the quasi-random band model under as many different but realistic conditions as possible by comparing the results of this model with available experimental and theoretical results. For several molecular species, experimental results for spectral transmittance and total band absorptance are given by Burch et al. (ref. 21) under different pressure and path length conditions. Thus, it is highly desirable to compare the results of the QRB model with these experimental results. For cases where experimental results are not available, it is important to compare the QRB results with LBL results. For certain spectral ranges and atmospheric conditions, results of atmospheric transmittances are available in the literature which have been obtained by using a sophisticated program called LOWTRAN (ref. 22). It is, therefore, desirable to obtain the QRB results exactly for these conditions for comparison with the LOWTRAN results. After these model validations, the aim of this study is to use the QRB model for evaluating the upwelling atmospheric radiance under different realistic surface and atmospheric conditions.

The basic formulation of the radiative transfer equations and the expressions for the upwelling radiance and flux are presented in the next section, "Basic Formulation." Details of the spectral models used in the study are given under "Evaluation of Transmittance and Integrated Absorption." The numerical procedure and data source for calculating the transmittance, total absorptance, and upwelling radiance are presented next ("Computational Procedure and Data Source"). Finally, results of the entire study are presented and discussed in "Results and Discussion."

LIST OF SYMBOLS

A	total band absorptance
$B(\omega,T)$	Planck function, W sec^{-1} sr^{-1} cm^{-2}
$Ch\ \phi$	Chapman function
$E(\omega)$	total radiant energy, W cm^{-2} sr^{-1}
$E_G(\omega)$	thermal radiation emitted by the underlying surface and atmosphere
$E_{GR}(\omega)$	reflected atmospheric radiation from the surface
$E_R(\omega)$	incident solar radiation reflected by the surface
$E_\phi(\omega)$	radiation scattered by single or multiple scattering processes in the atmosphere without having been reflected from the surface
$E_{R\phi}(\omega)$	scattered energy which has undergone a reflection from the surface
$f_j(\omega,\gamma_j)$	line shape factor for jth line
$H_S(\omega)$	Sun irradiance on the top of the atmosphere, W cm^{-2} sr^{-1}
I_ν	specific intensity
j_ν	emission coefficient
J_ν	nonequilibrium source function
P	total pressure
p	partial pressure
Q_{ij}	volume mixing ratio of the ith constituent in the jth layer, ppm V.
S_j	line strength of the jth line
$T(z)$	Atmospheric temperature, K
T_s	surface temperature, K
u	pressure path length, cm-atm
γ_j	half-width of the jth line
Δ	spectral range

Δ	subinterval in the spectral range
ε	surface emissivity
θ	Sun zenith angle
$\kappa(\omega)$	absorption coefficient
κ^D	direct contribution of absorption coefficient
κ^W	absorption coefficient in the wing region
κ_ν	frequency-dependent absorption coefficient
ν	frequency
ρ	density of the absorbing medium
$\tau(\omega,z)$	transmittance of the medium
ω	wave number, cm^{-1}

BASIC FORMULATION

Introduction

The fundamental quantities for describing the upwelling radiance are discussed in this section. Following the formulation of the equation of radiative transfer, the expression for thermal radiation emerging from a plane parallel atmosphere is presented.

Radiative Transfer Equation

The amount of radiant energy dE_ν, in a specified frequency interval $(\nu, \nu + d\nu)$, which is transported across an element of area da and in directions confined to an element of solid angle $d\omega$ during a time dt, is expressed in terms of intensity I_ν as:

$$dE_\nu = I_\nu \cos \theta \, d\nu \, da \, d\omega \, dt \tag{1}$$

where θ is the angle which the direction considered makes with the outward normal to da. With reference to figure 1, let us consider a small cylindrical element of cross-section da and height dz in the atmopshere. The radiation emerges into the atmosphere from the surface whose temperature is at T_s and the total thickness of the atmosphere is h. The difference in the radiative energy within the frequency interval ν and $\nu + d\nu$ crossing the two faces normally in a time dt and confined to an element of solid angle $d\omega$ is given by

$$\frac{dI_\nu}{ds} ds \, d\nu \, da \, d\omega \, dt \tag{2}$$

where ds is the thickness of the atmosphere in the direction of propagation of radiation. This difference in energy must arise from the excess of emission over absorption in the frequency interval of the solid angle considered.

The amount of energy absorbed is equal to

$$(\kappa_\nu \rho \, ds) \, (I_\nu \, d\nu \, da \, d\omega \, dt) \tag{3}$$

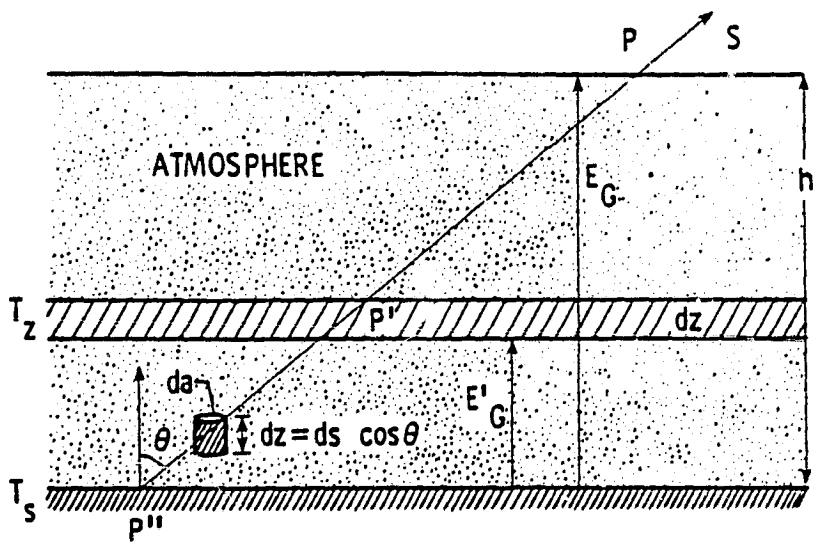

Figure 1. A stratified atmosphere.

Here ρ is the density of the absorbing medium and κ_ν is the frequency-dependent absorption coefficient.

The amount of energy emitted is given by

$$j_\nu \rho \, da \, ds \, d\omega \, dt \tag{4}$$

where j_ν is the emission coefficient.

Equating the gain and loss in the pencil of radiation, we have

$$dI_\nu/ds = - \kappa_\nu \rho \, I_\nu + j_\nu \rho \tag{5}$$

Equation (5) can be rewritten as

$$dI_\nu/ds = (J_\nu - I_\nu) \rho \, \kappa_\nu \tag{6}$$

where J_ν is the nonequilibrium source function.

Now consider a medium which is in local thermodynamic equilibrium. The absorption and emission of radiation is given by the Kirchoff's law

$$e_\nu = \kappa_\nu B_\nu \tag{7}$$

where B_ν is the Planck function and is given by

$$B_\nu = \frac{2\pi h \nu^3}{c^2[\exp (h\nu/\kappa T) - 1]} \tag{8}$$

Under such conditions, the transfer equation (6) becomes

$$dI_\nu/ds = (B_\nu - I_\nu) \rho \, \kappa_\nu \tag{9}$$

The total flux of radiation arriving at a point in the atmosphere (from above or below point) can be computed by integrating equation (9) as shown in reference 23.

Total Upwelling Radiance

The radiation emergent from the atmosphere is given by the expression (refs. 4, 24):

$$E(\omega) = E_G(\omega) + E_{GR}(\omega) + E_{\phi}(\omega) + E_{R\phi}(\omega) \tag{10}$$

where

$E_G(\omega)$ = thermal radiation emitted by underlying surface and atmosphere

$E_{GR}(\omega)$ = reflected atmospheric radiation from the surface

$E_R(\omega)$ = incident solar radiation reflected by the surface

$E_{\phi}(\omega)$ = the radiation scattered by single or multiple scattering processes in the atmosphere without having been reflected from the surface

$E_{R\phi}(\omega)$ = the scattered energy which has undergone a reflection from the surface

The various components of the upwelling radiation are pictorially shown in figure 2.

In the spectral region of infrared measurements, the effect of scattering and solar-reflected radiation is usually omitted. Hence, the expression for thermal radiation emerging from a plane parallel atmosphere can be written as

$$E(\omega) = E_G(\omega) + E_{GR}(\omega) = \varepsilon(\omega)\, B(\omega,T_s)\, \tau(\omega,0) + \int_0^h B[\omega,T(z)]\, [d\tau(\omega,z)/dz]\, dz + \rho(\omega)\, \bar{F}(\omega,T)\, \tau(\omega,0) \tag{11}$$

where $\varepsilon(\omega)$ is the surface emittance, $B(\omega,T)$ is the Planck function, T_s is the surface temperature, $T(z)$ is the temperature at altitude z, $\rho(\omega)$ is the diffuse surface reflectance, $\bar{F}(\omega,T)$ is the downward atmospheric radiation, and $\tau(\omega,0)$ and $\tau(\omega,z)$ are the transmittances from the top of the atmosphere to the surface and the altitude z, respectively. The first term on the right-hand side of equation (11) represents the radiation from the surface; the second term is the radiation from the atmosphere, and the third term represents the reflected component of the downward radiation.

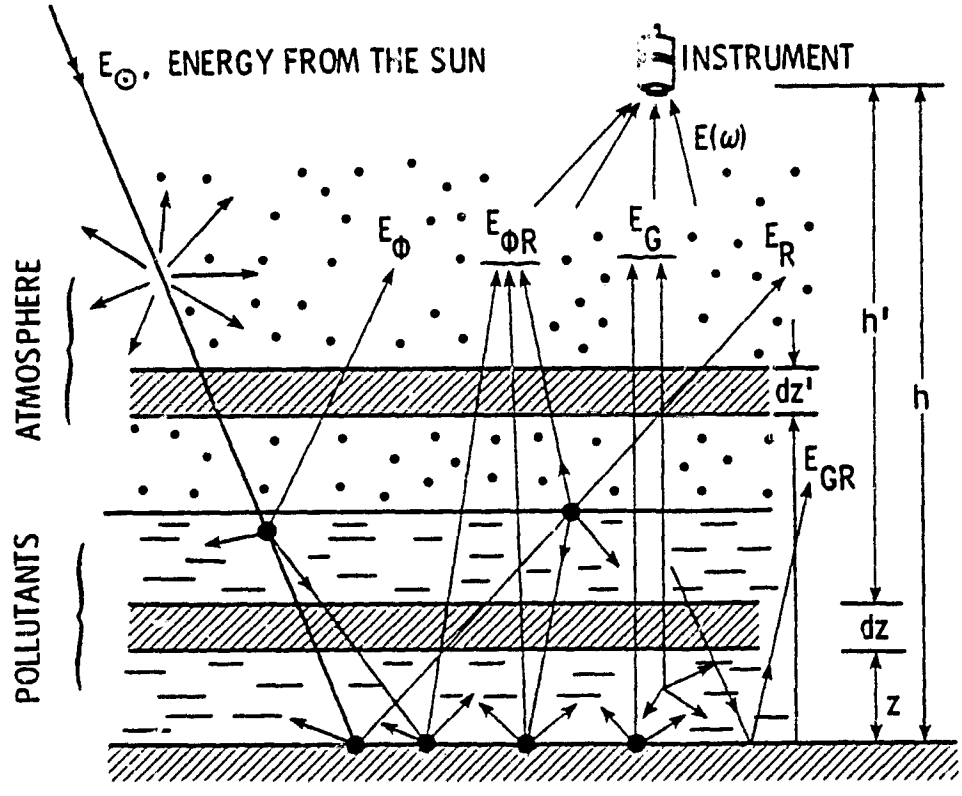

Figure 2. Various components of radiation received by an aircraft or satellite-mounted instrument.

Equation (11) can be obtained by integrating equation (9) in a manner described in reference 25. The contribution of the reflected atmospheric radiation from the surface is usually neglected for surfaces with relatively high values of surface emittance and for the spectral regions where the downward atmospheric emission is small.

The contribution of the sunlight reflected from the surface is important at shorter wave lengths and is given by the component $E_R(\omega)$ as

$$E_R(\omega) = \frac{1}{\pi} [1 - \varepsilon(\omega)] \cos \theta \, H_S(\omega) \, [\tau(\omega)]^{\chi} \tag{12}$$

where θ is the Sun's zenith angle, $[1 - \varepsilon(\omega)]$ is the ground reflectance of the surface, $H_S(\omega)$ is the Sun irradiance on the top of the atmosphere, $\chi = 1 + f(\theta)$ where $f(\theta) = \sec \theta$ for $0 \leq \theta \leq 60°$ and $\mathrm{Ch}\ \theta$ for $\theta > 60°$ with $\mathrm{Ch}\ \theta$ denoting Chapman's function, and $\tau(\omega) = \tau(\omega,0)$ is the transmission vertically through the atmosphere.

For radiation budget and cooling rate calculations, however, the required quantity is the flux density. Upward flux density can be obtained precisely by integrating the upwelling radiance over the zenith angle θ and the azimuth ϕ, such that

$$F(\omega,h) = \int_0^{2\pi} d\phi \int_0^{\pi/2} E(\omega,h) \sin \theta \cos \theta \, d\theta \tag{13}$$

Integration of equation (13) by using detailed angular distribution of radiance is a tedious problem. However, it is simplified considerably for a plane-parallel atmosphere and assuming that the source function in equation (11) is isotropic. It is possible with the above assumption to adapt the two-stream approximation whereby the equations of transfer are reduced to only two.

For the purpose of analysis (i.e., radiation modeling) and measurement of outgoing flux, it has been suggested to divide the entire long-wave spectral range into the following subregions (ref. 25):

(a) 0.7 to 4 μ

(b) 4 to 8 μ

(c) 8 to 12 μ

(d) 9 to 10 μ

(e) 12 to 18 μ

(f) 18 to 50 μ

Specific reasons for suggesting this spectral subdivision are given in reference 25. Different molecular bands and atmospheric effects are encountered in different spectral regions. Solar radiation absorption by H_2O and CO_2 occurs in the 0.7- to 4-μ region. Absorption by the 6.3-μ H_2O band is important in the 4- to 8-μ region. The effects of H_2O continuum bands, N_2O, chlorofluoromethanes and aerosols are important in the 8- to 12-μ region. The contribution of 9.6 μ O_3 is important in the 9- to 10-μ region. The combined effect of CO_2 and H_2O (but mostly CO_2) is important in the 12- to 18-μ region, and the effects of the H_2O pure rotation bands are important in the 18- to 50-μ region.

The greatest problem in computing heat fluxes is the integration of equation (11) or (13) over the frequency range of interest. The absorption coefficient (and, hence, the transmittance) is a highly variable function of the frequency, and for accurate work it should be evaluated at small frequency intervals. Furthermore, within a band which usually consists of thousands of rotational lines, the absorption coefficient at any frequency is made up of contributions from many lines. In principle, therefore, it is possible to calculate the absorption coefficient with very high accuracy by summing the contributions of all intervening lines. In practice, however, it is a very tedious and time-consuming process. For a wide frequency range with several bands, each with a large number of lines, large amounts of computer resources are required. As such, use of simplified but accurate models for spectral absorption is highly desirable. Considerable efforts have been spent in the past in devising simplified models to overcome the problem of numerical integration over the complicated line structure of the atmospheric spectrum. A complete review on different absorption models is available in reference 4. The absorption models used in the present study are discussed in the next section.

EVALUATION OF TRANSMITTANCE AND INTEGRATED ABSORPTANCE

Introduction

Accurate calculation of the atmospheric transmittance is important for the correct evaluation of the atmospheric radiative heat flux. In cases where high spectral resolutions are desired, the actual distribution of line positions and intensities become important, and the contributions from the wings of distant lines need to be included. In such cases, a line-by-line model should be employed (refs. 4, 19, 20). If the integrated signals are measured over relatively wide spectral intervals, an appropriate band model could be employed. A brief description of the spectral models used in this study is presented in this section.

In order to describe the infrared absorption characteristics of a radiating molecule, it is necessary to consider the variation of the spectral absorption coefficient for a single line. In general, for a single line centered at the wave number ω_j, this is expressed as

$$\kappa_{\omega j} = S_j \, f_j(\omega, \gamma_j) \tag{14}$$

where S_j is the intensity of the jth spectral line and is given by

$$S_j = \int_{-\infty}^{\infty} \kappa_{\omega j} \, d(\omega - \omega_j) \tag{15}$$

The quantity $f_j(\omega - \omega_j)$ is the line shape factor for the jth spectral line. It is a function of the wave number and the half-width γ_j and is normalized on $\omega - \omega_j$ such that

$$\int_{-\infty}^{\infty} f_j(\omega - \omega_j) \, d(\omega - \omega_j) = 1 \tag{16}$$

Several approximate line profiles have been described in the literature. The most commonly used profiles are rectangular, triangular Lorentz, Doppler, or Voigt (combined Lorentz and Doppler) profiles. The study of line shapes and line broadening is an active research field. For various reviews on the

subject, one should refer to references 26 to 31. Lorentz, Doppler, and Voigt profiles are of special interest in the atmospheric studies, and these are discussed in some detail in reference 4. The line profile usually employed for studies of infrared radiative transfer in the Earth's atmosphere is the Lorentz pressure-broadened line shape; the shape factor for which is such that the absorption coefficient is expressed as

$$\kappa_{\omega j} = S_j \gamma_j / \pi [(\omega - \omega_j)^2 + \gamma_j^2] \tag{17}$$

where γ_j represents the Lorentz line half-width. From simple kinetic theory it may be shown that γ_j varies with pressure and temperature according to the relation

$$\gamma_j = \gamma_{jo} (P/P_o)^m (T_o/T)^n \tag{18}$$

where γ_{jo} is the line half-width corresponding to a reference temperature, T_o and a pressure P_o. The values of m and n depend, in general, on the collision parameters and on the nature of the molecules. The values of $m = 1$ and $n = 0.5$ are employed for most atmospheric studies.

The radiative transmittance at any wave number ω is given by the relation

$$\tau_\omega = \exp\left(-\int_0^u \kappa_\omega \, u\right) \tag{19}$$

where κ_ω is the absorption coefficient at ω per cm-atm and u represents the pressure path length of the absorber in cm-atm. An appropriate spectral model for the absorption coefficient is employed to calculate the transmittance from equation (19). The total absorption of a single line in an infinite spectral interval is given by

$$A_j = \int_{-\infty}^{\infty} (1 - \tau_{\omega_j}) \, d(\omega - \omega_j) \tag{20}$$

For a homogenous path, this can be expressed as

$$A_j = \int_{-\infty}^{\infty} [1 - \exp(-\kappa_{\omega j} u)]\, d(\omega - \omega_j) \tag{21}$$

It should be noted that the integration in equations (20) and (21) extends only to the spectral range of a single line.

The spectral absorptance of a narrow band (consisting of a sufficiently large number of spectral lines) may be expressed by

$$A_\omega = 1 - \tau_\omega = 1 - \exp(1 - \int_0^u \kappa_\omega\, du) \tag{22}$$

For a homogenous path, the total absorptance of a narrow band is given by

$$A = \int_{\Delta\omega} A_\omega\, d\omega = \int_{\Delta\omega} [1 - \exp(-\kappa_\omega u)] d\omega \tag{23}$$

where limits of integration are considered over the narrow band pass. The total band absorptance of a wide band may, in turn, be expressed by

$$A = \int_{-\infty}^{\infty} [1 - \exp(-\kappa_\omega u)]\, d(\omega - \omega_o) \tag{24}$$

where the limits of integration are considered over the entire band pass and ω_o is the wave number at the center of the wide band. A brief description of the LBL and QRB models and a few relations for the total band absorptance are presented in the following subsections.

Line-by-Line (LBL) Model

For a homogeneous path, the monochromatic transmittance as given by equation (19) becomes

$$\tau(\omega) = \exp[-\kappa(\omega)\, u] \tag{25}$$

The value of the absorption coefficient at the wave number due to direct and wing contributions is given by

$$\kappa(\omega) = \kappa^D(\omega) + \kappa^W(\omega) \tag{26}$$

where $\kappa^{D}(\omega)$ and $\kappa^{W}(\omega)$ represent the direct and wing contributions respectively. The lines whose centers fall close to the wave number under consideration are treated as directly contributing lines. The direct contribution from lines of Lorentz shape is given by equation (17). The wing contributions to $\kappa(\omega)$ are from lines located far from the wave number under consideration. The absorption coefficient in the wing region is calculated from the relation

$$\kappa^{W}(\omega) = \sum_{j} \left\{ S_j \gamma_j / [\pi(\omega - \omega_j)^2] \right\} \qquad (27)$$

In the present study, the Lorentz LBL model is used in calculating the transmittance values in certain cases for comparison with the QRB model results.

Quasi-Random Band (QRB) Model

The QRB model, introduced by Wyatt et al. (ref. 10), is one of the best models available for evaluating the transmittance and absorption of a vibration-rotation band. The use of this model in transmittance calculation results in a considerable reduction in computational time. The procedure for calculating transmittance by the QRB model is discussed here. A listing of the computer program is given in Appendix A, and various symbols used in the program are explained in Appendix B.

In this method, the entire frequency range Δ is divided into a number of small subintervals δ of equal spectral width. The lines in each of these smaller intervals are assumed to be arranged in a random manner. The average transmittance over the entire spectral range is obtained by averaging the transmittances of all subintervals. By considering the intensity of the strongest line, five intensity groups are created. Thus, lines whose intensities are within 10^{-5} times the intensity of the strongest line are taken into consideration. The expression for the transmission can be written as

$$\tau(\omega,z) = \exp\left[-\int_{0}^{x} \sum_{i} \kappa_i^m(\omega,x)\, \rho_i(x)\, dx\right] \qquad (28)$$

where $\kappa_i^m(\omega,x)$ is the mass absorption coefficient for the ith absorbing gas, ρ_i is the mass density, and x is the depth of the level measured from the top of the atmosphere. Equation (28) can be changed into an alternate form as

$$\tau(\omega,z) = \exp[-\int_0^u \sum_i \kappa_i(\omega)du_i \tag{29}$$

where

$$\kappa(\omega) = \kappa^m(\omega)\ (\rho_r/\rho_g) \tag{30}$$

$$du = P_g\ (\rho_g/\rho_r)dx \tag{31}$$

and P_g is the partial pressure, ρ_g is the mass density of the absorber, and ρ_r is the absorber density corresponding to reference condition (STP).

The average transmittance due to a single spectral line over the subinterval δ may be expressed as

$$\tau(\omega) = \frac{1}{\delta}\int_\delta \exp[-S_j\ u\ f\ (\omega,\omega_j)]d\omega_j \tag{32}$$

The average transmittance, τ_d, due to all the lines in that decade is given as

$$\tau_d(\omega) = \left\{\frac{1}{\delta}\int_\delta \exp[-\overline{S}_j\ u\ f\ (\omega,\omega_j)]d\omega_j\right\}^N \tag{33}$$

where N is the number of lines within the decade and $\overline{S}_j$ is the average intensity of all the lines within the decade. The average transmittance due to all lines in the five intensity decades of subinterval δ is expressed by

$$\tau_\kappa(\omega) = \prod_{d=1}^{5}\left\{\frac{1}{\delta\kappa}\int_{\delta\kappa} \exp[-\overline{S}_j\ u\ f\ (\omega,\omega_j)]d\omega_j\right\}^N \tag{34}$$

where k represents the kth subinternal of total span Δ. Further information on this model can be obtained from reference 12.

Exponential Sum Fit Method

Numerous approximate methods have been developed for calculating spectrally integrated radiative flux. These methods completely avoid the cumbersome procedure of taking care of exact line strengths and line shapes. One such method is the exponential sum fitting of transmissions (ESFT). This method which has evolved recently is based on the fitting of the transmission function averaged over a spectral interval $\Delta\omega$ by a sum of exponentials (ref. 13). The ESFT has been used for evaluating the total band absorptance of water vapor bands.

The empirical relations for total band absorptance of 0.94, 1.38, 1.87, 2.7, 3.2, and 6.3 μ water vapor bands have been obtained by Howard et al. (ref. 32). These relations were obtained by curve fitting the experimental results. The experimental results were represented by two separate relations as

$$A = \int_{\Delta\omega} A_\omega \, d\omega = cu^{1/2}(P + p), \quad A < A_c \tag{35}$$

$$A = \int_{\Delta\omega} A_\omega \, d\omega = C + D \log u + K \log (P + p), \quad A > A_c \tag{36}$$

In the above relations, u is the absorber concentration in gm $\cdot$ cm^{-2}, P is the total pressure in mm Hg, and p is the partial pressure of H_2O in mm Hg. The quantities c, k, C, K and D are the empirically determined constants, and A_c is the absorption above which the strong band relation [eq. (36)] becomes applicable. It has been found by Liou and Sasamori (ref. 33) that the above relations are not continuous when $A = A_c$. They have modified these relations, and the absorptivity from the laboratory measurements has been fitted into a single relation as

$$\bar{A} = \frac{A}{\Delta\omega} = \frac{1}{\Delta\omega}\left[C + D \log_{10} (x + x_o)\right] \tag{37}$$

where $x = uP^{K/D}$, $x_o = 10^{-C/D}$

The values of the constants c, k, C, D, K, A_c and x are given by Liou and Sasamori (ref. 33). The total absorption of each band is fitted by a series of exponential functions

$$A = \Delta\omega\left[1 - \sum_{m=1}^{M} w_n \exp(-k_n x)\right] \tag{38}$$

where w_n and k_n are the exponential fit parameters, independent of atmospheric conditions, and M is the number of divisions in a particular band. The exponential fit parameters k_n and w_n have been obtained by Stephens (ref. 34) by fitting the total band absorption of each band into the relation of equation (38). The constant w_n and k_n are tabulated in reference 34 for the water vapor bands.

Empirical Relations for Carbon Dioxide Band Absorptance

The empirical relations for total band absorption of the carbon dioxide bands have been obtained by fitting experimental results in the equation by Howard et al. (ref. 35):

$$\int A_\omega \, d\omega = c u^{1/2} (P + p)^k \tag{39}$$

where u is the CO_2 absorber concentration, P is the total pressure, p is the partial pressure of CO_2, and c is a constant. It has been shown by many investigators that the total absorption of the CO_2 band varies as $u^{1/2}$. It has been shown that total absorption is proportional to $(P + p)^k$ where k varies from 1/2 to 1/4. The above expression is valid only for weak bands. The empirical expression for the total absorption of the strong band is given by the following equation

$$\int A_\omega \, d\omega = C + D \log u + K \log (P + p) \tag{40}$$

where C, D, and K are constants. For small values of total band absorptance, most of the bands follow the "weak band" relation [eq. (39)], and for large values of total band absorptance the "strong band" relation [eq. (40)] is followed. Most of the bands have "transition values" of total absorption above which equation (40) applies and below which equation (39) applies.

In the present study, the empirical results have been compared with the experimental as well as QRB model results only for the 2.7-μ CO_2 band. The various constants used in the above relations are given in reference 35.

Computer Code LOWTRAN

The computer code LOWTRAN has been developed to calculate atmospheric transmittance over a broad spectral interval, the 0.25- to 28.5-μ region (ref. 15). This method has been based on an empirical graphical prediction scheme. The transmittance is calculated by LBL calculations and averaged over a spectral interval of 20 cm^{-1}. This transmission data, over a wide spectral range and for a wide range of atmospheric paths, has been calculated and presented in different charts in reference 36. The atmospheric transmittance for various spectral intervals and atmospheric paths can be predicted from these charts. The LOWTRAN is a computer code where all the spectral curves, transmittance functions, etc. have been digitalized. This program is very versatile and transmittance can be computed for six different types of atmosphere.

COMPUTATIONAL PROCEDURE AND DATA SOURCE

The numerical procedure for evaluating the spectral atmospheric transmittance and the upwelling radiance and the data source used for the calculations are described briefly in this section. The first step involved in accurate calculation of the transmittance is the evaluation of the spectral absorption coefficient. Use of equation (17) is made in evaluating the absorption coefficient values.

In calculating the atmospheric transmittance, the atmosphere is divided into a number of layers of equal thickness (in the present case, 1 km). For the present study, the top of the atmosphere was considered to be 10 km, which is approximately the top of the troposphere. The pressure path length is given by the expression

$$du_{ij} = Q_{ij}(P_j/P_{NTP})\ (T_{NTP}/T_j)dzj \tag{41}$$

where Q_{ij} is the volume mixing ratio of the ith constituent in the jth layer, dzj is the thickness of the jth layer, and P_j and T_j are the pressure and temperature at the center of the jth layer, respectively. The transmittance at location z in the atmosphere is given by

$$\tau(\omega,z) = \exp[-\int_0^u \sum_j \sum_i \kappa_{ij}(\omega)du_{ij} \tag{42}$$

Following the procedure for evaluating the atmospheric transmittance, upwelling radiance is calculated by dividing the nonhomogenous atmosphere into a number of homogenous sublayers. If the gas molecules absorb in a specified spectral region $\Delta\omega$, then the upwelling radiance is given by

$$E = \int_{\Delta\omega} E_\omega\, d\omega \tag{43}$$

Equation (11) is used for calculating the upwelling radiance E in the present study.

The line parameters needed for this study (position, strength, line, width, etc.) were obtained from McClatchey et al. (ref. 36, 37). The "McClatchey Tape" is available at the NASA/Langley Research Center. The

atmospheric temperature and pressure profiles were taken from the U.S. Standard Atmosphere 1962 (ref. 38). The concentration distributions in the atmosphere for H_2O, CO_2, N_2O and O_3 were taken from McClatchey et al. (ref. 36). The CO_2 and N_2O are assumed to be uniformly mixed in the atmosphere. Rotational and vibrational partition functions, required to account for the temperature dependence of the line strengths, were taken from McClatchey et al. (ref. 37).

RESULTS AND DISCUSSION

Introduction

Spectral transmittance and total band absorptance of selected molecular bands (1.87-μ H_2O, 2.7-μ CO_2, 2.73-μ H_2O, 4.5-μ N_2O, and 7.66-μ CH_4) are evaluated by using the QRB model. For a few cases, LBL procedure is also used in calculating the transmittance. The results are compared with available experimental results. Similar comparisons for some other molecular bands are available in reference 20. The total band absorptance calculated by using the ESFT method and empirical correlations are compared with the experimental as well as QRB model results for the H_2O and CO_2 bands.

Atmospheric transmittances are evaluated for selected spectral ranges of the longwave region by using the QRB model, and these are compared with the LOWTRAN results. Finally, the results for upwelling radiance, calculated by using the QRB model, are presented to emphasize the use of the QRB model for actual atmospheric applications.

Transmittance and Total Band Absorptance

The spectral transmittance and total band absorptance results are presented in this section for different molecular bands. These results have been obtained by assuming a homogenous medium with constant pressure path lengths. This is because experimental results were available only for homogenous conditions. The results obtained under actual atmospheric conditions are presented in the next section. It should also be pointed out here that LBL and QRB model results have been obtained for exactly the same conditions (physical and spectral) for which experimental results were available. As such, transmittance results for certain bands may not be spectrally symmetric.

7.66-μ CH_4 band. - The spectral variation of the transmittance, as calculated by the QRB and/or LBL models, is illustrated in figures 3 and 4 for two different pressures but for the same pressure path length. The experimental results for exactly the same conditions are also shown in these figures for comparison. The overall agreement between these results is seen to be quite good. The transmittance values shown in figure 4 for

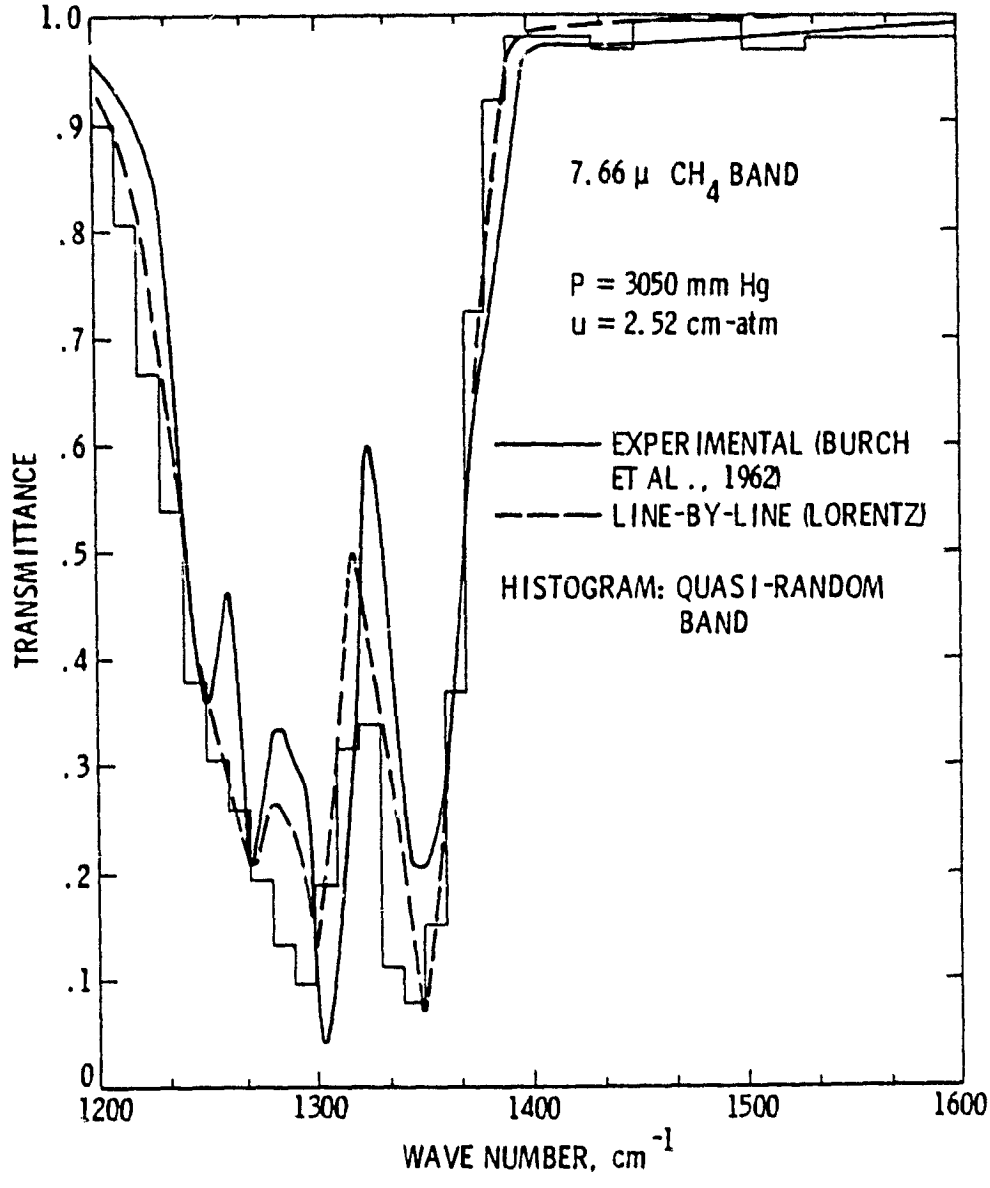

Figure 3. Comparison of transmittances of 7.66-μ CH_4 band (P = 3050 mm Hg, u = 2.52 cm-atm).

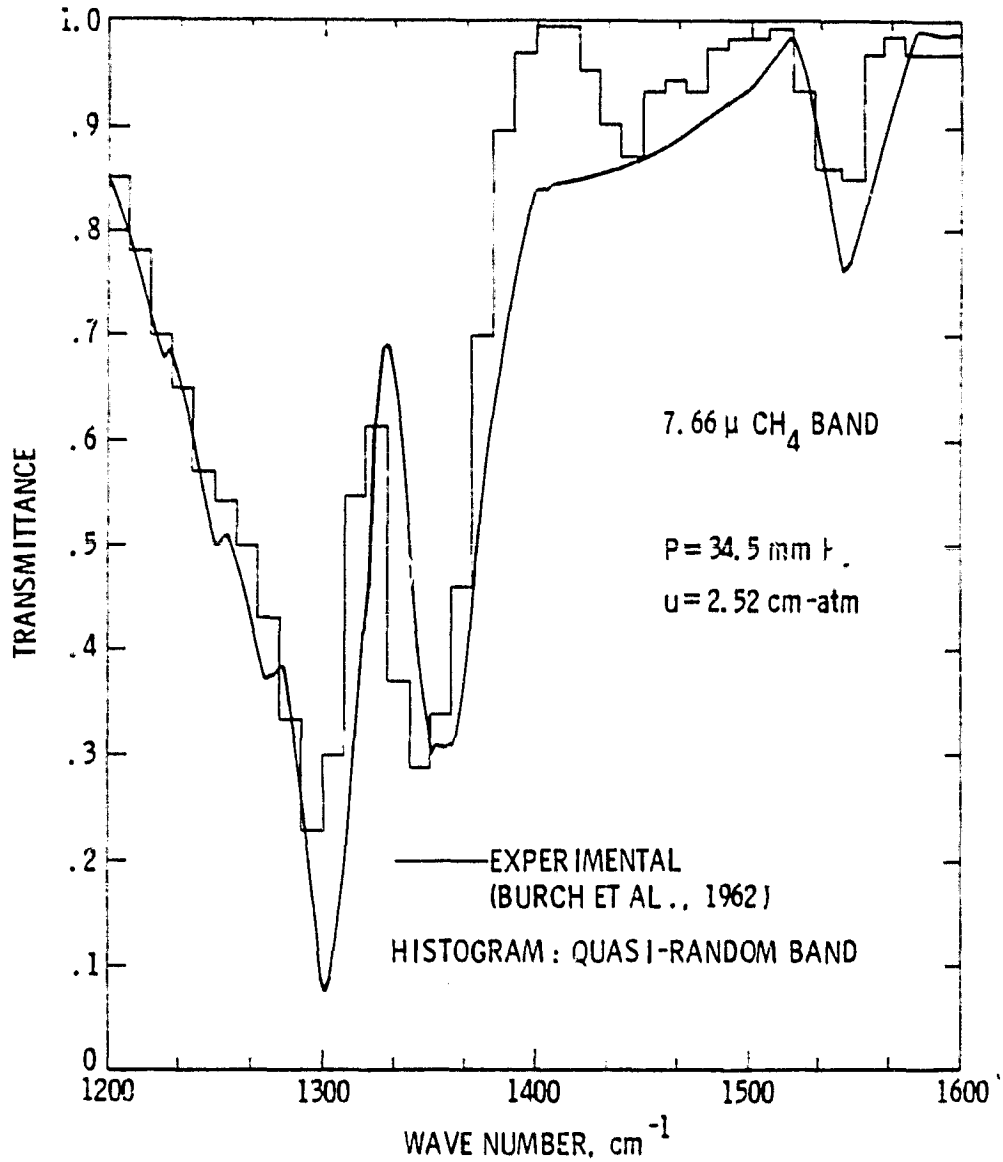

Figure 4. Comparison of transimttances of 7.66-μ CH_4 band (P = 34.5 mm Hg, u = 2.52 cm-atm).

a lower pressure are higher than the values shown in figure 3. This is especially true in the center portion of the band. This is because, for a fixed path length, absorption usually increases with the pressure until the large pressure limit is achieved. At this point, the central portion of the band becomes opaque and radiation absorption occurs only in the band wings. At lower pressures, however, absorption of radiation occurs in the entire band pass.

The total (or integrated) band absorptance results are illustrated in figure 5 as a function of pressure path length for three different pressures. For lower pressures (P = 50 and 200 mm Hg), the agreement between the QRB and experimental results is seen to be very good for all path lengths. For the moderate pressure of P = 300 mm Hg, however, the results are seen to be significantly different in the range of intermediate path lengths. It is possible that in this range the QRB model accounts for the absorption in the band wings more so than the experimental measurement. If results were available for sufficiently high pressures, only small differences between the two results would be noticed. This is because at sufficiently large pressure the central portion of the band becomes saturated. Although it is not convenient to show the limiting (linear and logarithmic) results in figure 5, it is noted that all the results tend to approach the linear limit toward the small path length and the logarithmic limit toward the large path length. Some comparative results for band absorptance are given in table 1. These results also exhibit the general trend seen in figure 5. It is noted from the results of the table at P = 3050 mm Hg that for this band the limit of large pressure will be reached at sufficiently high pressure.

4.5-μ N_2O band. - The variation of spectral transmittance with wave number is shown in figures 6 and 7 for two different pressures but the same pressure path length. The transmittance results have been calculated by the QRB as well as LBL model, and are compared with the experimental results. The agreement between the results is seen to be good over the entire band pass.

The band absorptance (i.e., the total band absorptance) results are illustrated in figures 8(a) and 8(b) for different pressures. Except for the results at P = 10 mm Hg, a general agreement between the QRB and

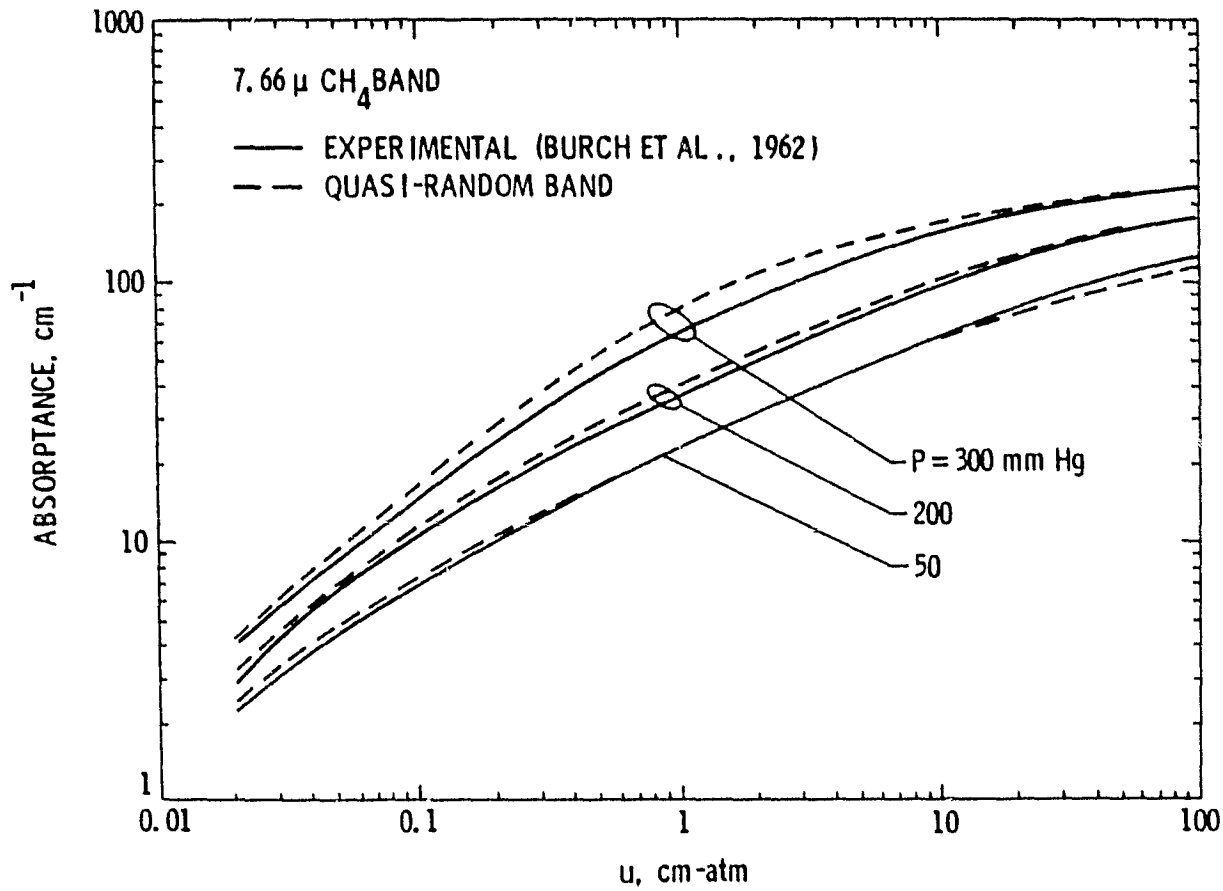

Figure 5. Comparison of total band absorptance of 7.66-μ CH_4 band.

Table 1. Comparison of total band absorptance for the 7.66-μ CH_4 band.

P (mm Hg)	u (cm-atm)	A_E (cm^{-1})	A_Q (cm^{-1})	$(A_E - A_Q)/A_E$ (%)
3054	2.52	102.0	119.2	-16.7
301	2.52	61.7	70.4	-14.1
55.5	2.52	35.0	37.8	-8.0
34.5	47.30	115.0	99.2	13.7

$A_E = \int A\, d\omega$ (Exp); $A_Q = \int A\, d\omega$ (QRB).

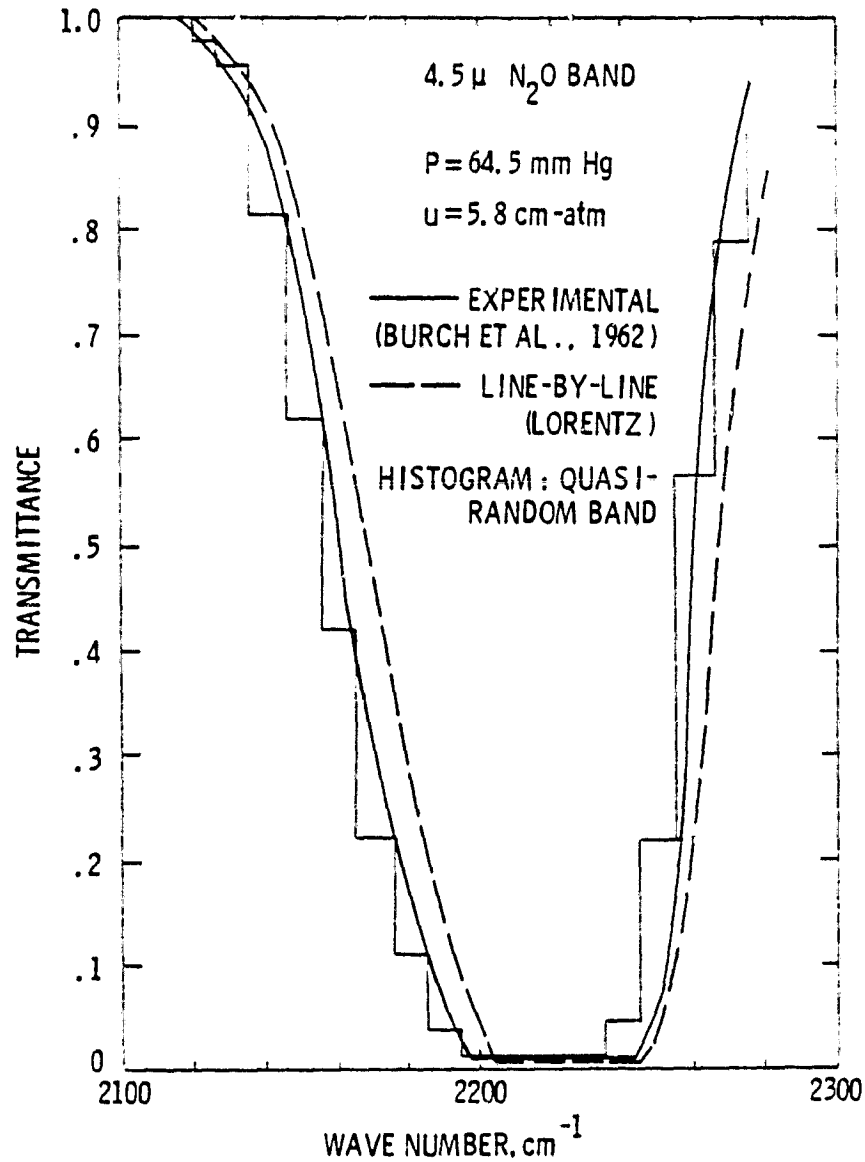

Figure 6. Comparison of transmittances of 4.5-μ N_2O band (P = 64.5 mm Hg, u = 5.8 cm-atm).

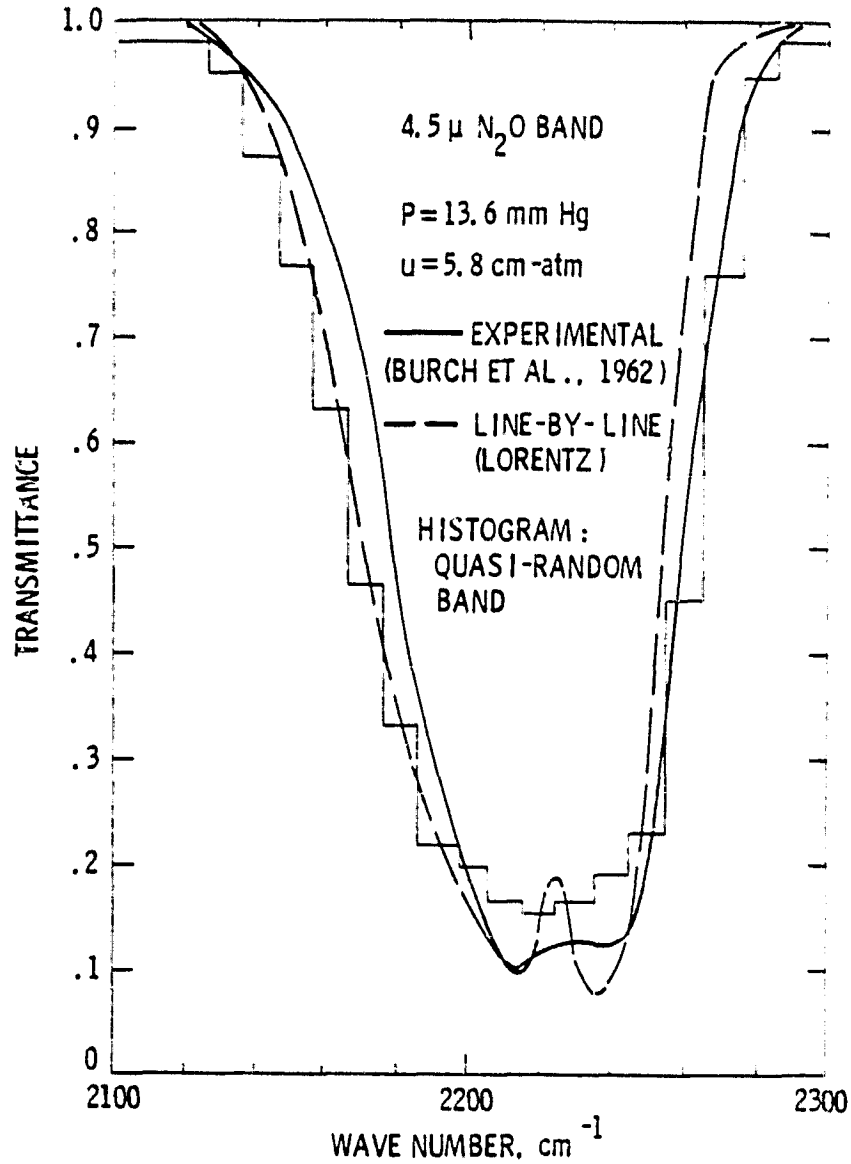

Figure 7. Comparison of transmittances of 4.5-μ N_2O band (P = 13.6 mm Hg, u = 5.8 cm-atm).

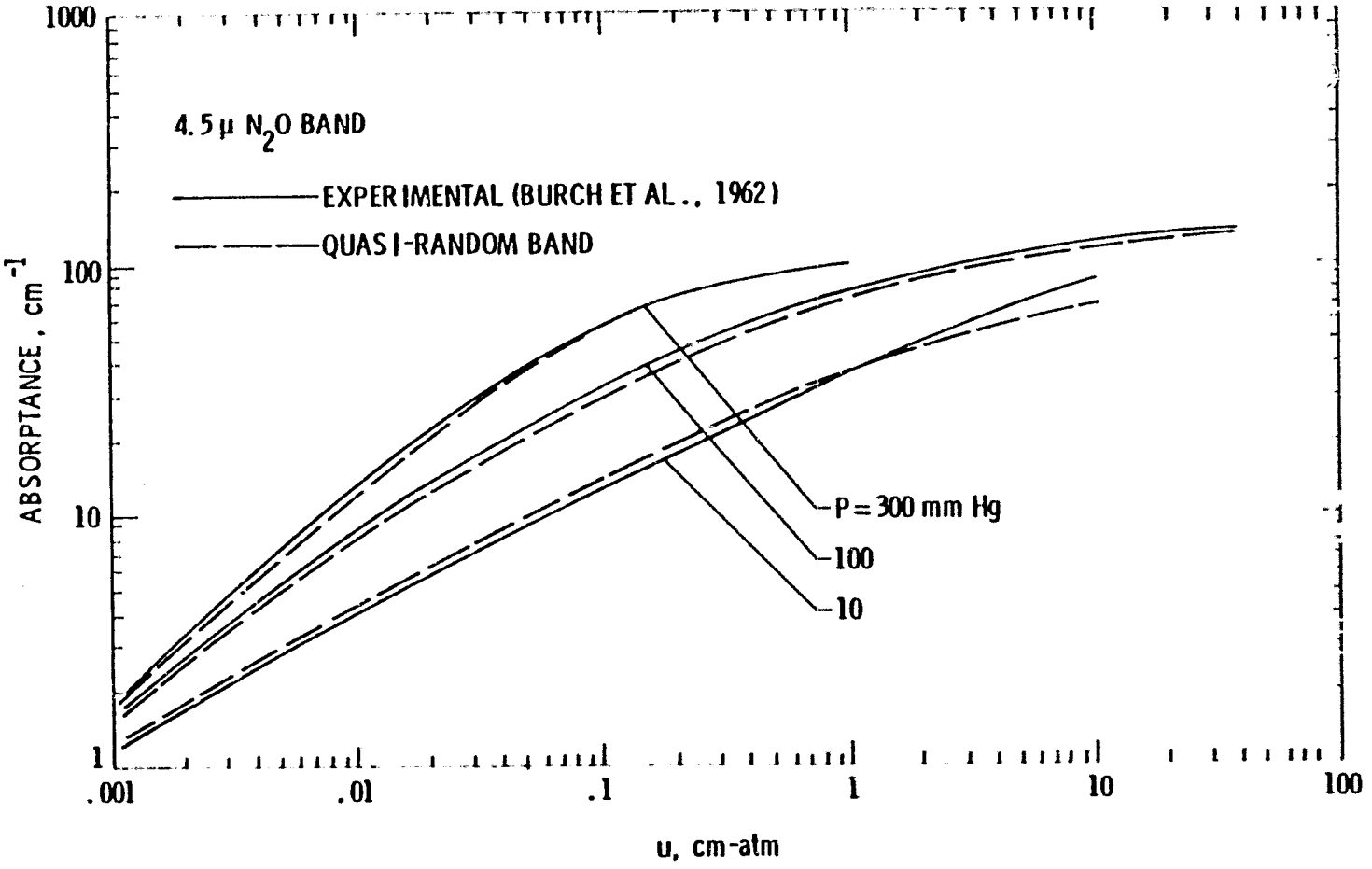

(a)

Figure 8. Comparison of total band absorptance of 4.5-μ N_2O band.

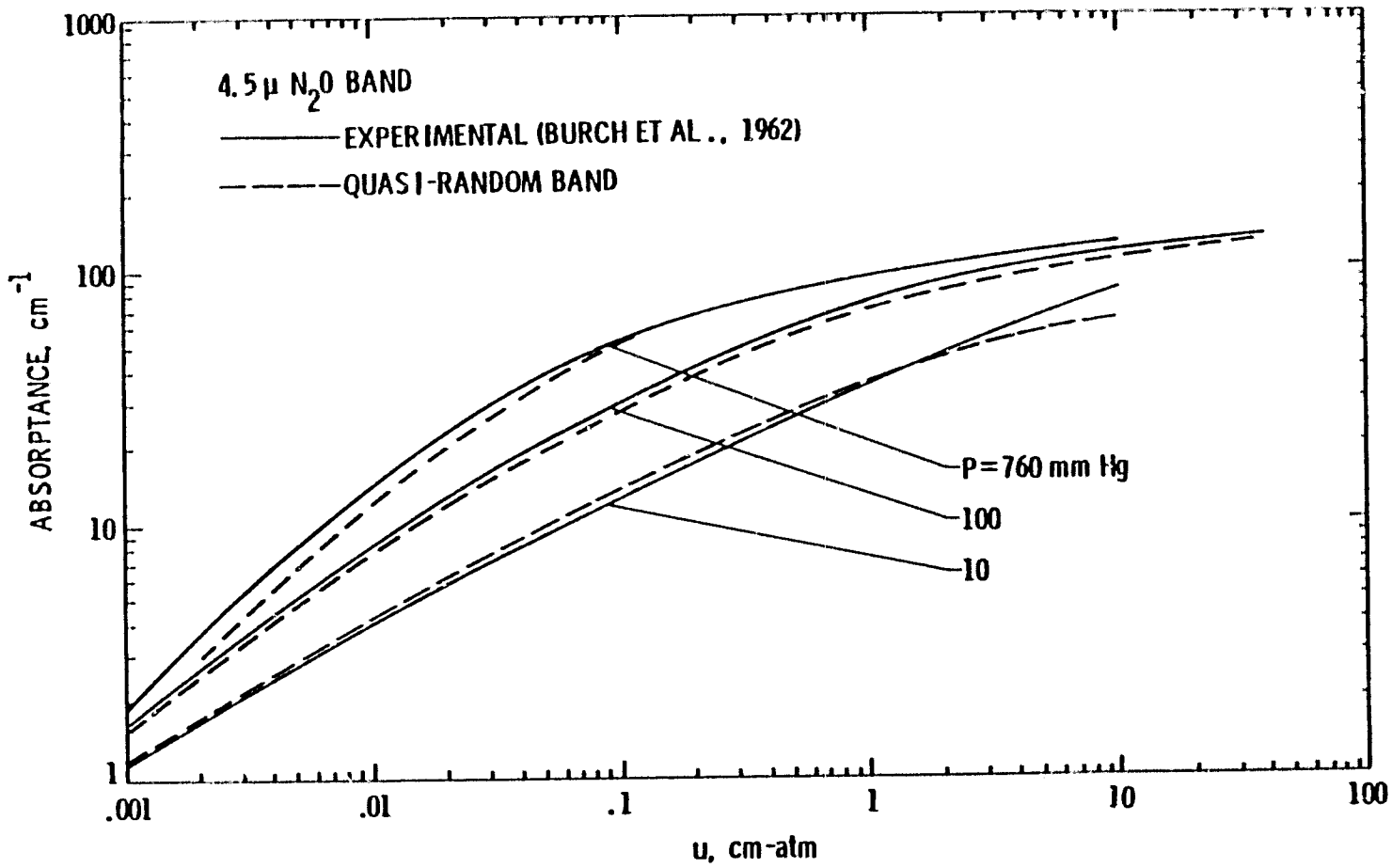

(b)

Figure 8. (Concluded).

experimental results is noted for all pressures at all path lengths. It is further noted that the results for P = 760 mm Hg and P = 3000 mm Hg are almost identical for the entire pressure path lengths. This indicates that for this band the limit of large pressure is reached for any pressure higher than P = 760 mm Hg. For this band, the band absorptance results are also given in table 2 for certain pressure and path length conditions. In most cases, the QRB and experimental results are found to be in very good agreement.

2.73-μ H_2O band. - The spectral transmittance results of the QRB model are compared with the experimental results in figure 9 for P = 862 mm Hg and u = 0.101 pr cm. The agreement between the results is seen to be excellent over the entire band pass.

The total band absorptance results calculated by using the QRB model and ESFT relation, equation (38), are compared with the experimental results in figure 10 for P = 20, 250, and 760 mm Hg. The QRB and ESFT results are seen to be in good agreement with the experimental results at higher pressures (P > 250 mm Hg). For P = 760 mm Hg, the QRB and ESFT results are found to be almost the same as the experimental results. A similar trend is also seen from the band absorptance results presented in table 3. As such, for this band, use of either the QRB model or the ESFT relation would be justified at higher pressures (above 250 mm Hg). For P = 20 mm Hg, however, a considerable difference between the experimental and ESFT results is noted for all path lengths, but virtually no difference is seen between the QRB and experimental results. The use of the ESFT relation, therefore, is not recommended for this band at lower pressures. The QRB model, on the other hand, could be employed at all pressure and path length conditions.

1.87-μ H_2O band. - The spectral transmittance results, as calculated by the QRB model, are compared with experimental results in figures 11 and 12 for 2 different pressures but for the same pressure path lengths of u = 0.101 pr cm. The agreement between the results is seen to be very good for the entire spectral range of the band. It is noted that, in the central portion of the band, the transmittance values are lower for the higher pressure (fig. 11), but they are relatively higher for the lower pressure (fig. 12). This, however, would be expected because at higher pressures the absorption is higher.

Table 2. Comparison of total band absorptance for the 4.5-μ N_2O band.

P (mm Hg)	u (cm-atm)	A_E (cm^{-1})	A_E (cm^{-1})	$(A_E - A_Q)/A_E$ (%)
750	5.8	113.4	119	-4.9
419	0.677	85.2	83.8	1.6
241	0.389	69.3	66	3.9
197	5.8	108.5	110.5	-1.8
69.4	0.112	28.2	27.7	1.7
64.5	5.8	100	100	0
56.2	0.091	24.7	23.2	6
35.3	0.057	20.2	15.4	23
26.7	5.8	91.6	87.8	4.1
21.8	0.0352	10.9	10.05	7.8
13.9	5.8	79.9	77	3.6

$A_E = \int A \, d\omega$ (Exp); $A_Q = \int A \, d\omega$ (QRB)

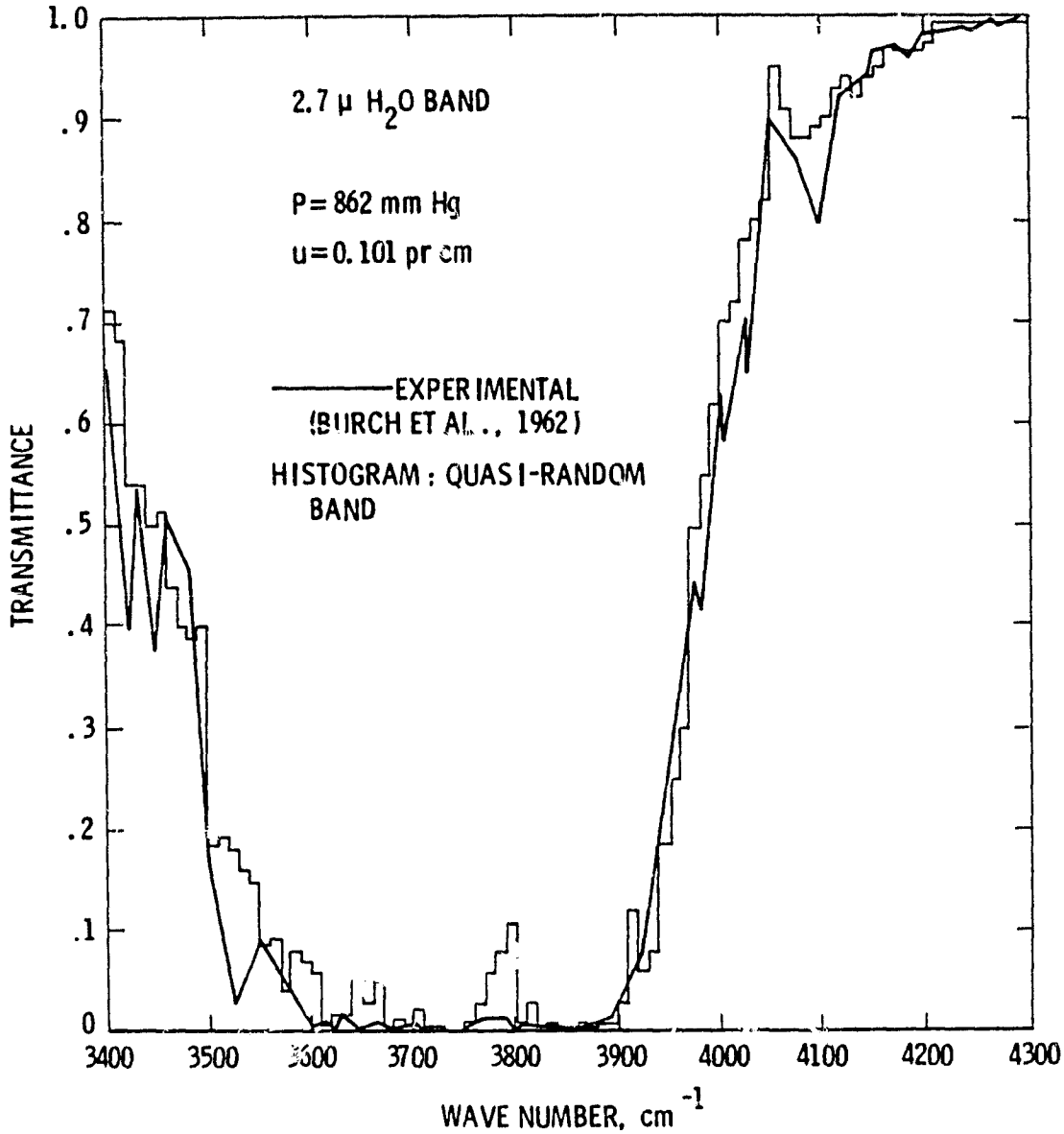

Figure 9. Comparison of transmittances of 2.7-μ H_2O band (P = 862 mm Hg, u = 0.101 pr cm).

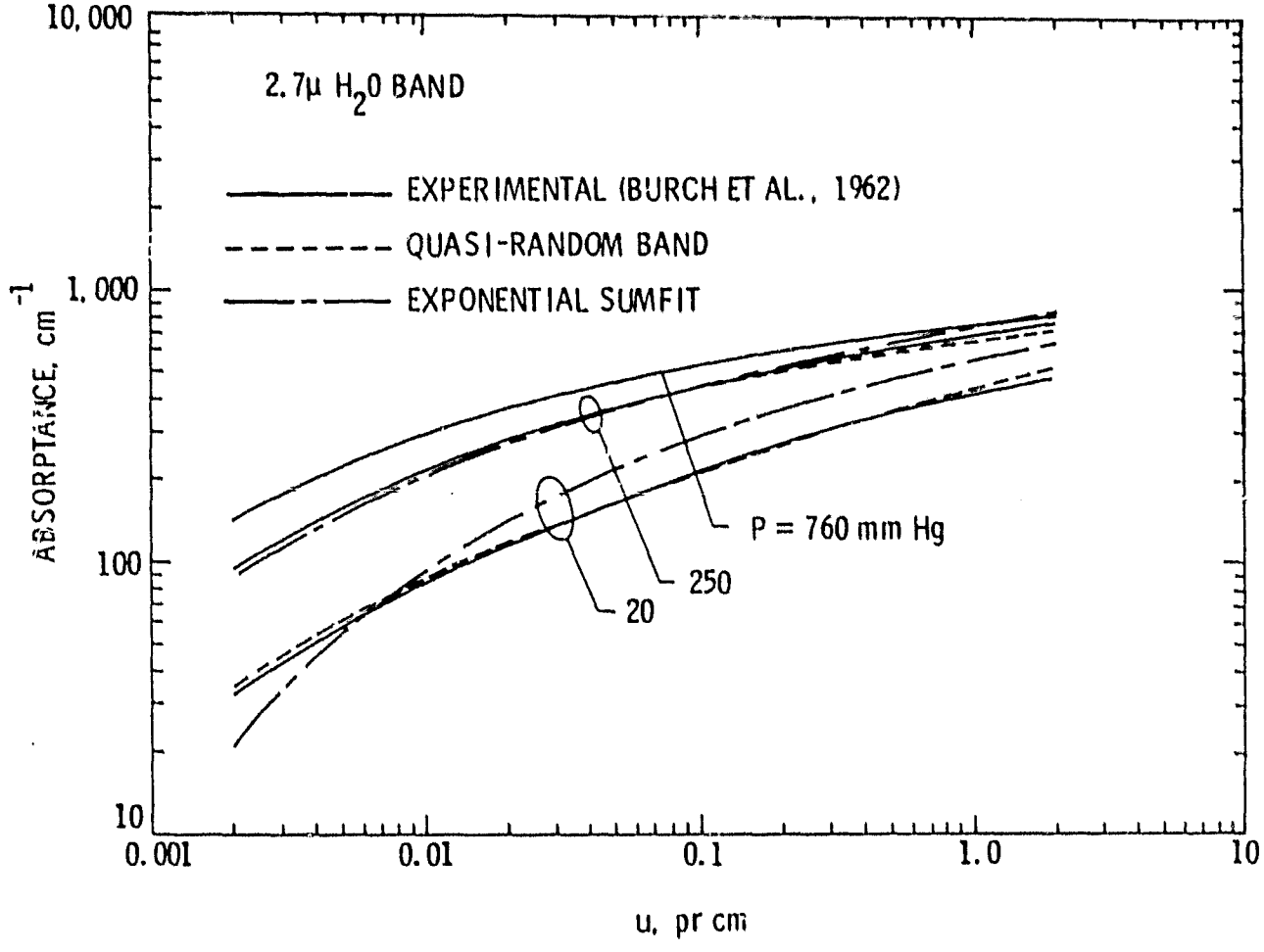

Figure 19. Comparison of total band absorptance of 2.7-u H_2O band.

Table 3. Comparison of total band absorptance for the 2.73-μ H_2O band.

P (mm Hg)	u (pr cm)	A_E (cm^{-1})	A_Q (cm^{-1})	A_S (cm^{-1})	$(A_E-A_Q)/A_E$ (%)	$(A_E-A_S)/A_E$ (%)
852	0.101	534	542	540	-2.3	-1.1
392	0.101	492	487	488	1.0	0.8
348	0.0524	417	406	411	2.6	1.4
208	0.101	449	430	447	4.2	0.4
170	0.0508	354	335	362	5.3	-2.2
87.5	0.0495	292	270	317	7.5	-8.6

$A_E = \int A\, d\omega$ (Exp); $A_Q = \int A\, d\omega$ (QRB); $A_S = \int A\, d\omega$ (ESFT).

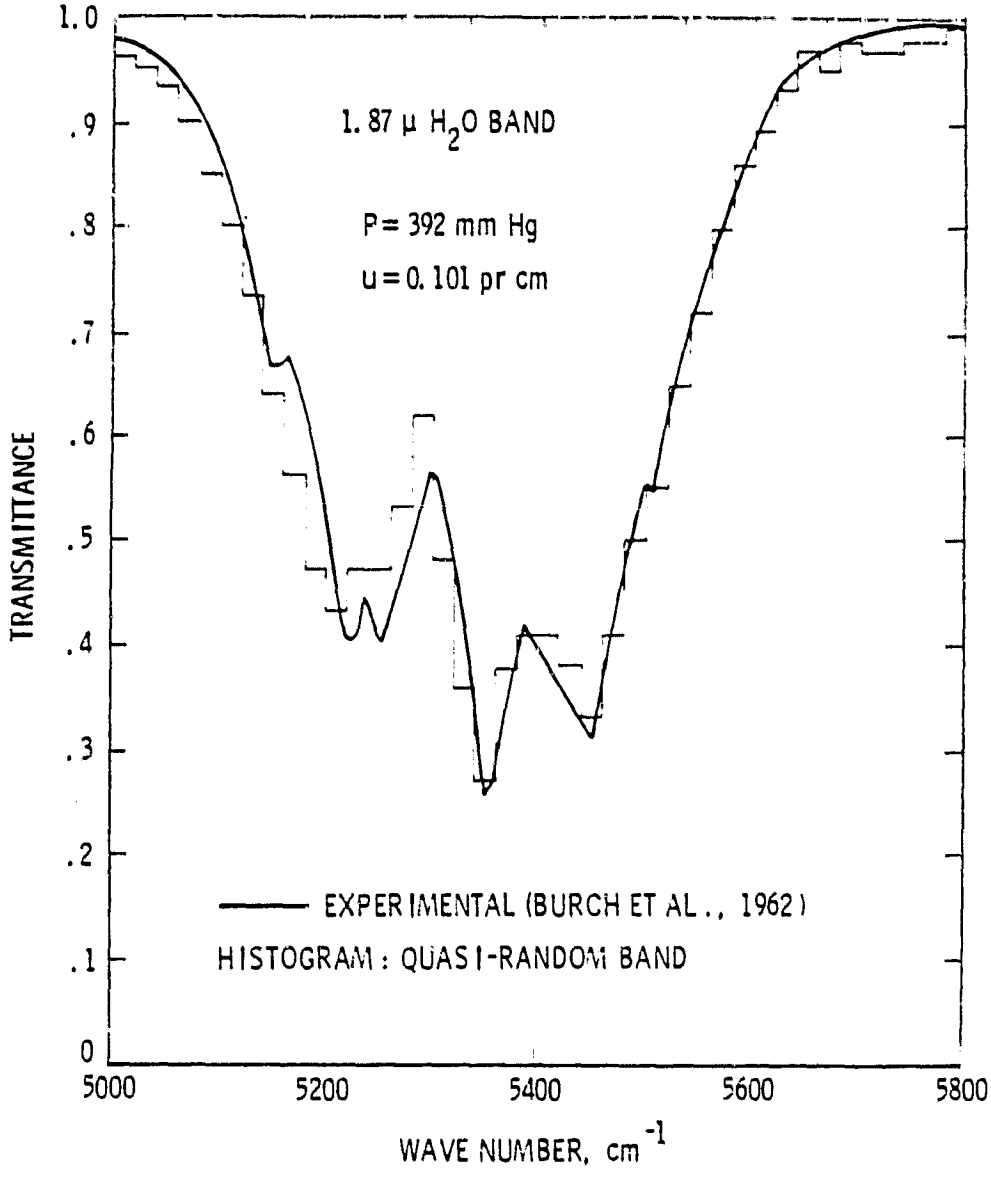

Figure 11. Comparison of transmittances of 1.87-u H_2O band (P = 392 mm Hg, u = 0.101 pr cm).

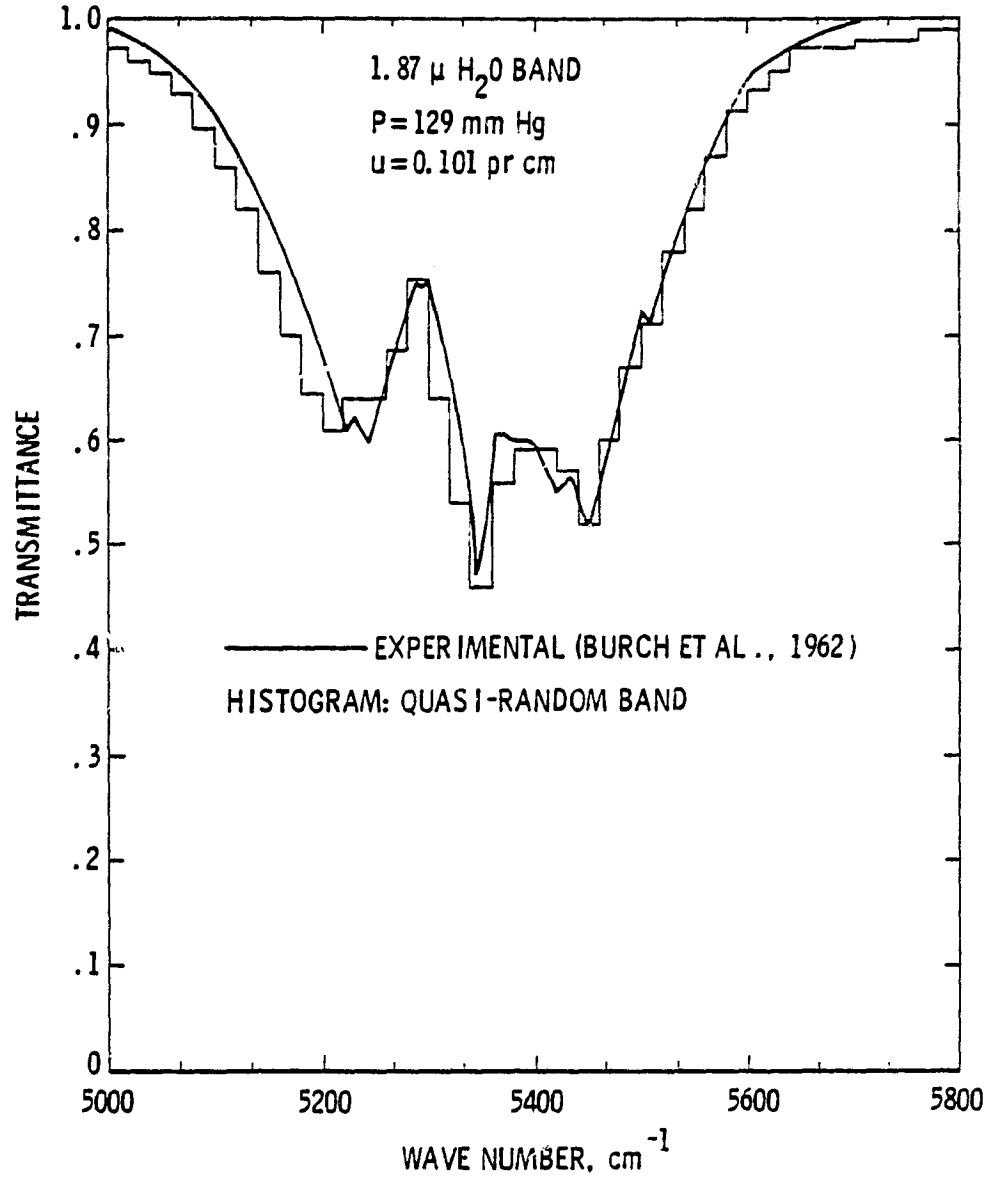

Figure 12. Comparison of transmittances of 1.87-u H_2O band (P = 129 mm Hg, u = 0.101 pr cm).

The band absorptance results, as calculated by the QRB model and ESFT relation, are compared with the experimental results in figure 13 for P = 40, 250, and 760 mm Hg. The agreement between the experimental and ESFT results is seen to be poor for all pressures and path lengths. This conclusion may also be derived from the band absorptance results presented in table 4. As such, use of the ESFT relation is not recommended for this band at atmospheric conditions. The use of the QRB model, however, could be made (with reasonable accuracy) for this band also.

2.7-μ CO_2 band. - The transmittance results of the QRB model are compared with the experimental results in figures 14 and 15 for two different pressures and path lengths. In general, the agreement between the results is good. It is obvious from the results of these figures that for higher pressures the transmittance values are lower because of higher absorption.

The band absorption results of the QRB model are compared with the experimental results in figure 16 for two different pressures (P = 100 and 760 mm Hg). The results are seen to be in excellent agreement for all path lengths. The band absorptance results have been calculated by the empirical correlations available for this band, and the results are tabulated in table 5 along with other results. From a comparison of the results presented in this table, it should be obvious that use of these correlations cannot be recommended for most atmospheric applications.

Atmospheric Transmittance

The atmospheric transmittance is evaluated by the QRB model as well as by the LOWTRAN Program. The results have been obtained for four different spectral ranges, and these are illustrated in figures 17 to 21. For this comparative study the top of the atmosphere was considered to be at 10 km, and all the results were obtained for the standard atmospheric conditions.

The results for the spectral range from 3300 to 3700 cm^{-1} are shown in figure 17. The contributions of all the important molecular bands in this spectral range (2.73-μ H_2O, 2.7-μ CO_2, 2.87-μ N_2O, and 2.97-μ N_2O) were considered in calculation of the transmittance. The QRB results are seen to be in general agreement with the LOWTRAN results.

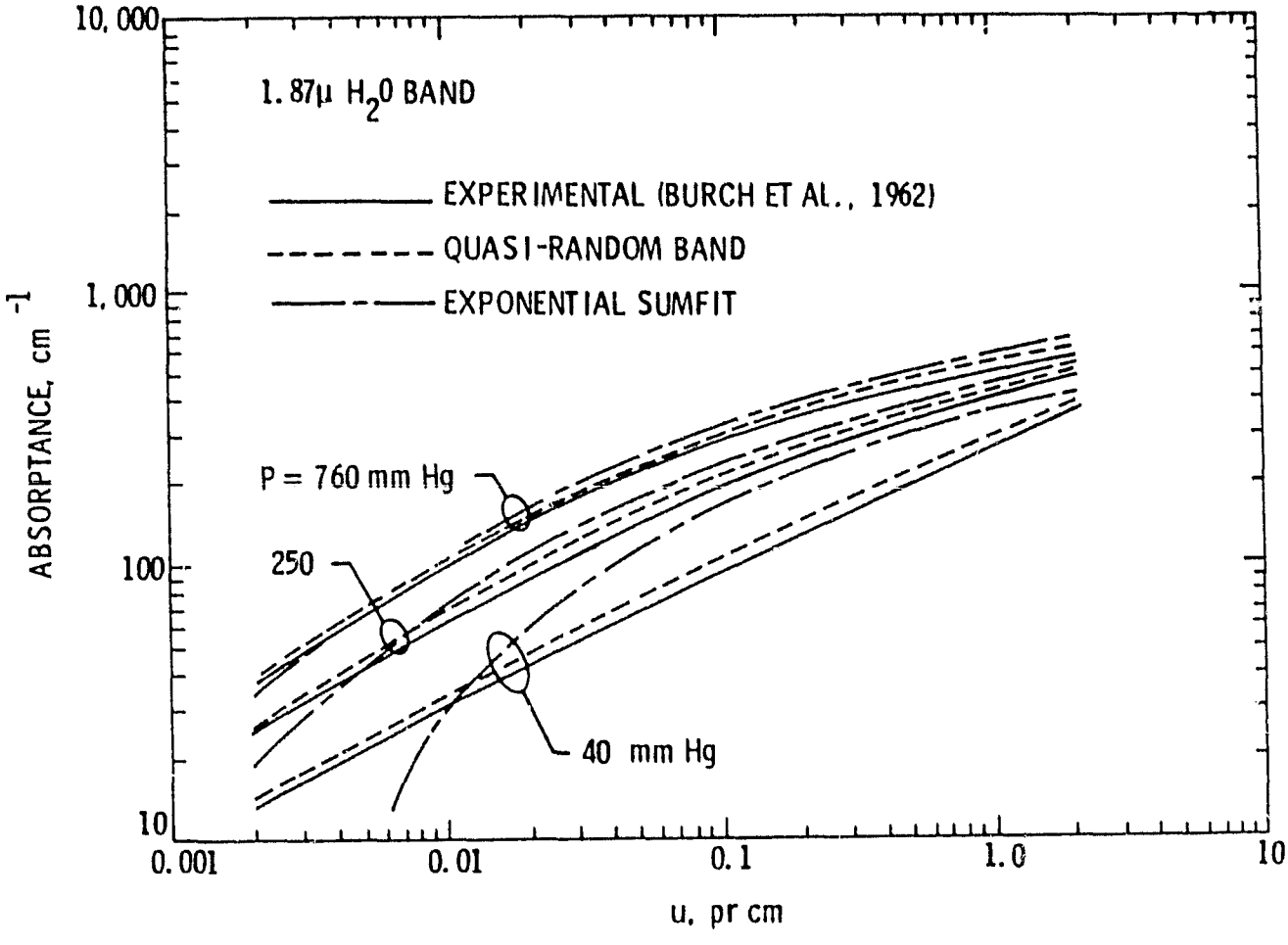

Figure 13. Comparison of total band absorptance of 1.87-μ H_2O band.

Table 4. Comparison of total band absorptance of the 1.87-μ H_2O band.

P (mm Hg)	u (pr cm)	A_E (cm^{-1})	A_Q (cm^{-1})	A_S (cm^{-1})	$(A_E-A_Q)/A_E$ (%)	$(A_E-A_S)/A_E$ (%)
862	0.101	299	309	322	-3.3	-7.7
765	0.0483	204	224	245	-9.8	-20
392	0.101	234	249	275	-6.4	-17.5
208	0.101	186	203	239	-9.1	-28
170	0.0509	120	139	168	-15.8	-40
129	0.101	153	171	212	-11.8	-38.6
113	0.109	151	168	212	-11.3	-40.4
88.8	0.0496	90.5	107	134	-18.2	-48

$A_E = \int A\, d\omega$ (Exp); $A_Q = \int A\, d\omega$ (QRB); $A_S = \int A\, d\omega$ (ESFT).

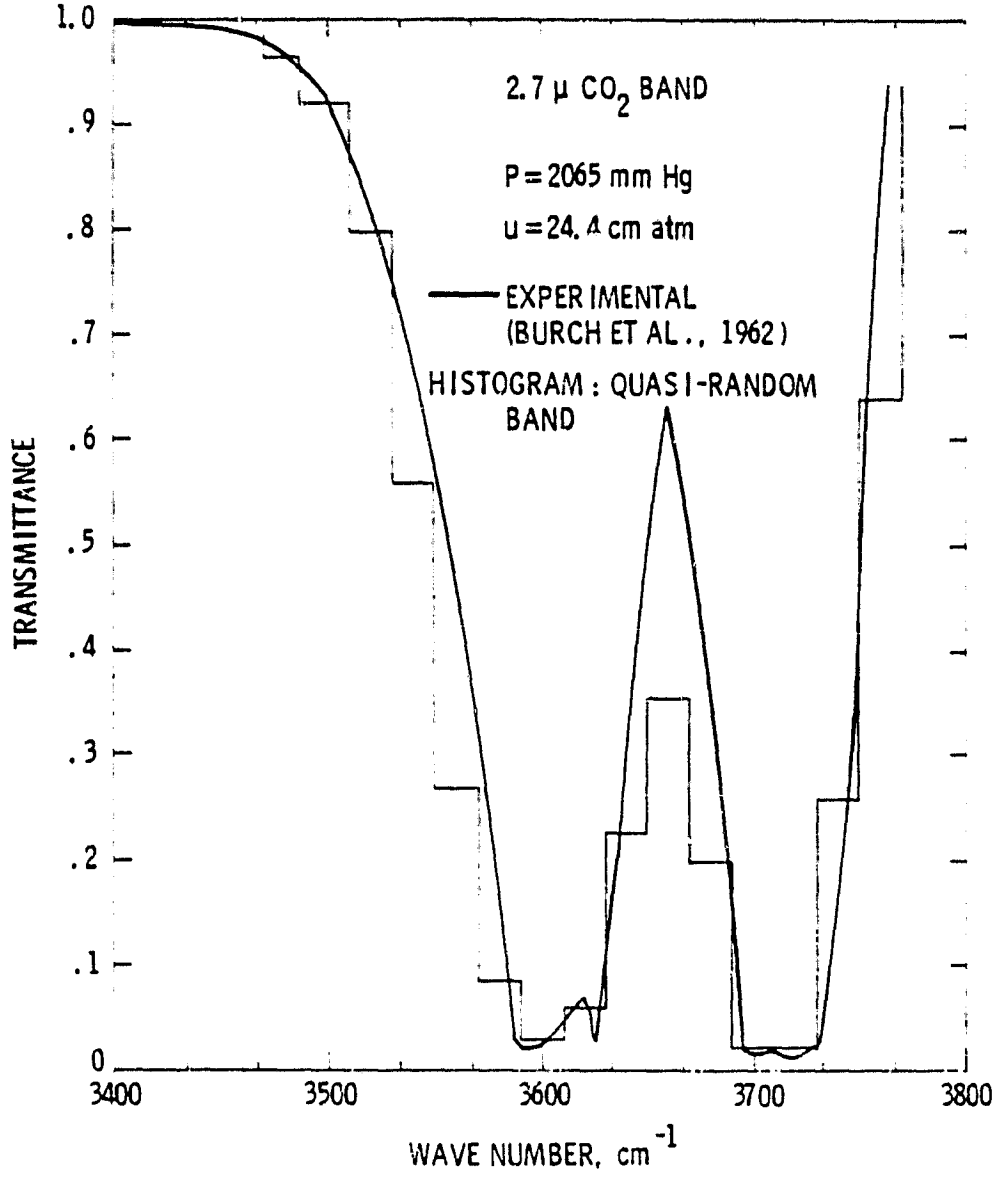

Figure 14. Comparison of transmittances of 2.7-μ CO_2 band (P = 2065 mm Hg, u = 24.4 cm-atm).

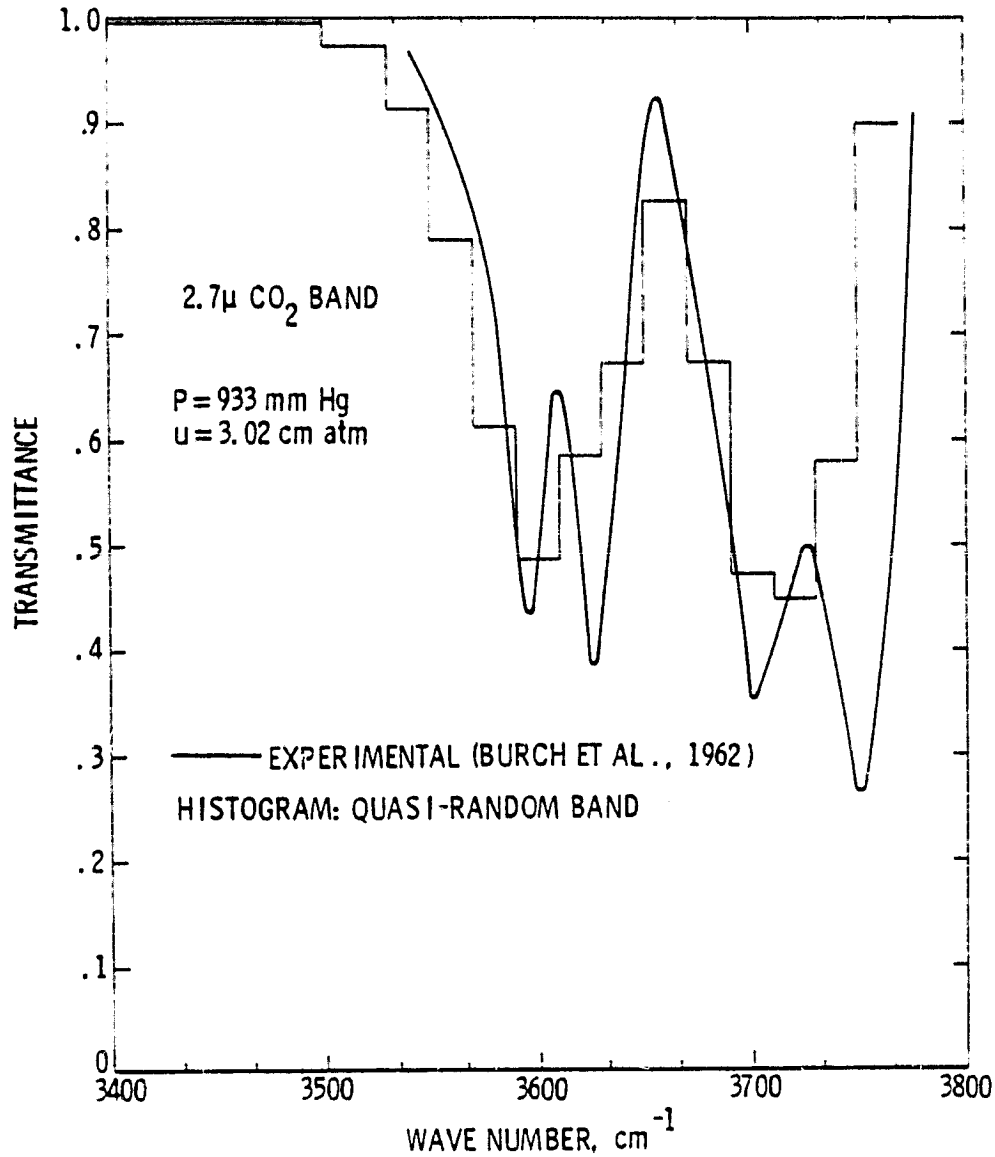

Figure 15. Comparison of transmittances of 2.7-μ CO_2 band (P = 933 mm Hg, u = 3.02 cm-atm).

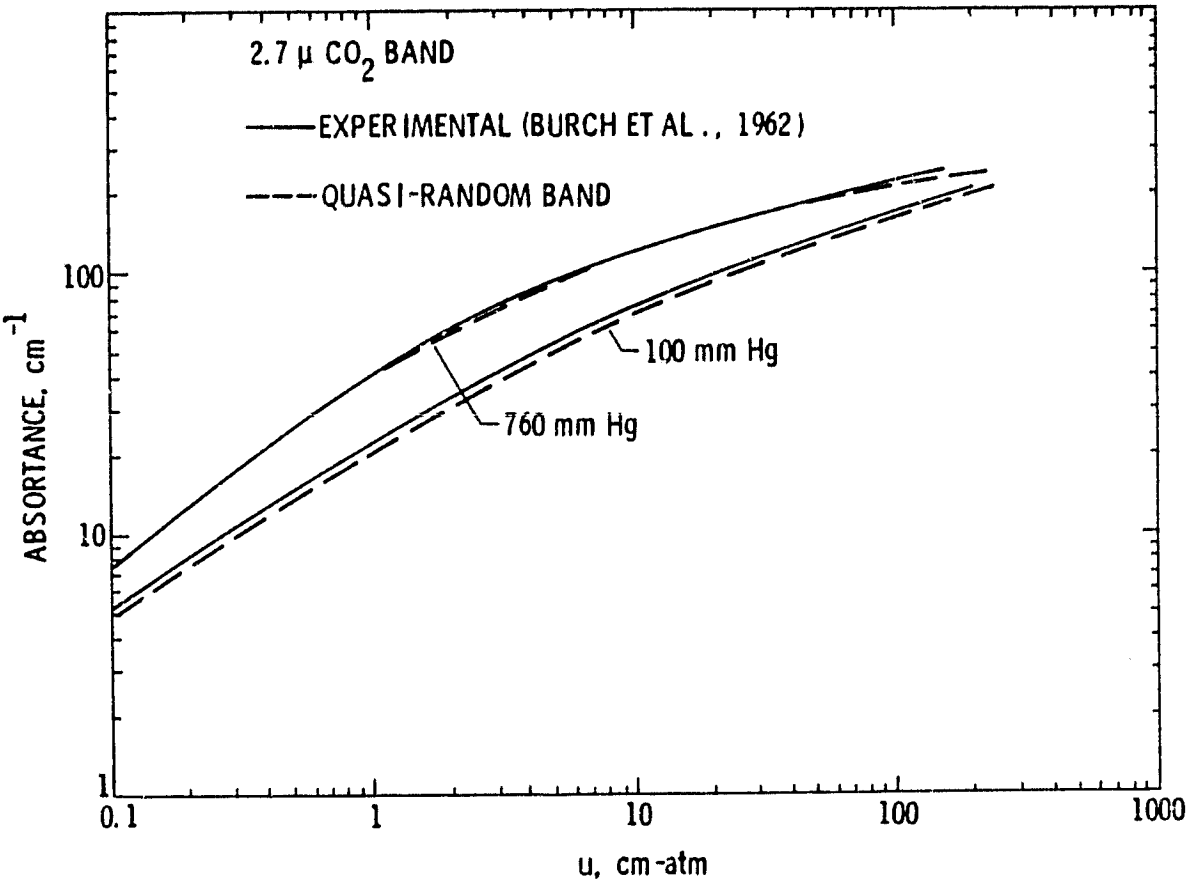

Figure 16. Comparison of total band absorptance of 2.7-u CO_2 band.

Table 5. Comparison of total band absorptance for the 2.7-μ CO_2 band.

P (mm Hg)	u (cm-atm)	A_E (cm^{-1})	A_Q (cm^{-1})	A_R (cm^{-1})	$(A_E-A_Q)/A_E$ (%)	$(A_E-A_R)A/E$ (%)
2065	24.4	179	189	195	-5.5	-8.9
1565	0.672	39.9	39.8	61	0.25	-52
933	3.02	83.9	81.0	102	3.4	-21
844	0.316	20.4	20.6	32	-0.9	-56
821	1.38	50.9	52.9	72	-3.9	-41.5
439	1.34	42.6	43.2	49.9	-1.4	-17
44.8	0.316	8.4	8.8	9.08	-4.7	-8

$A_E = \int A\, d\omega$ (Exp); $A_Q = \int A\, d\omega$ (QRB): $A_R = \int A\, d\omega$ (Correlation)

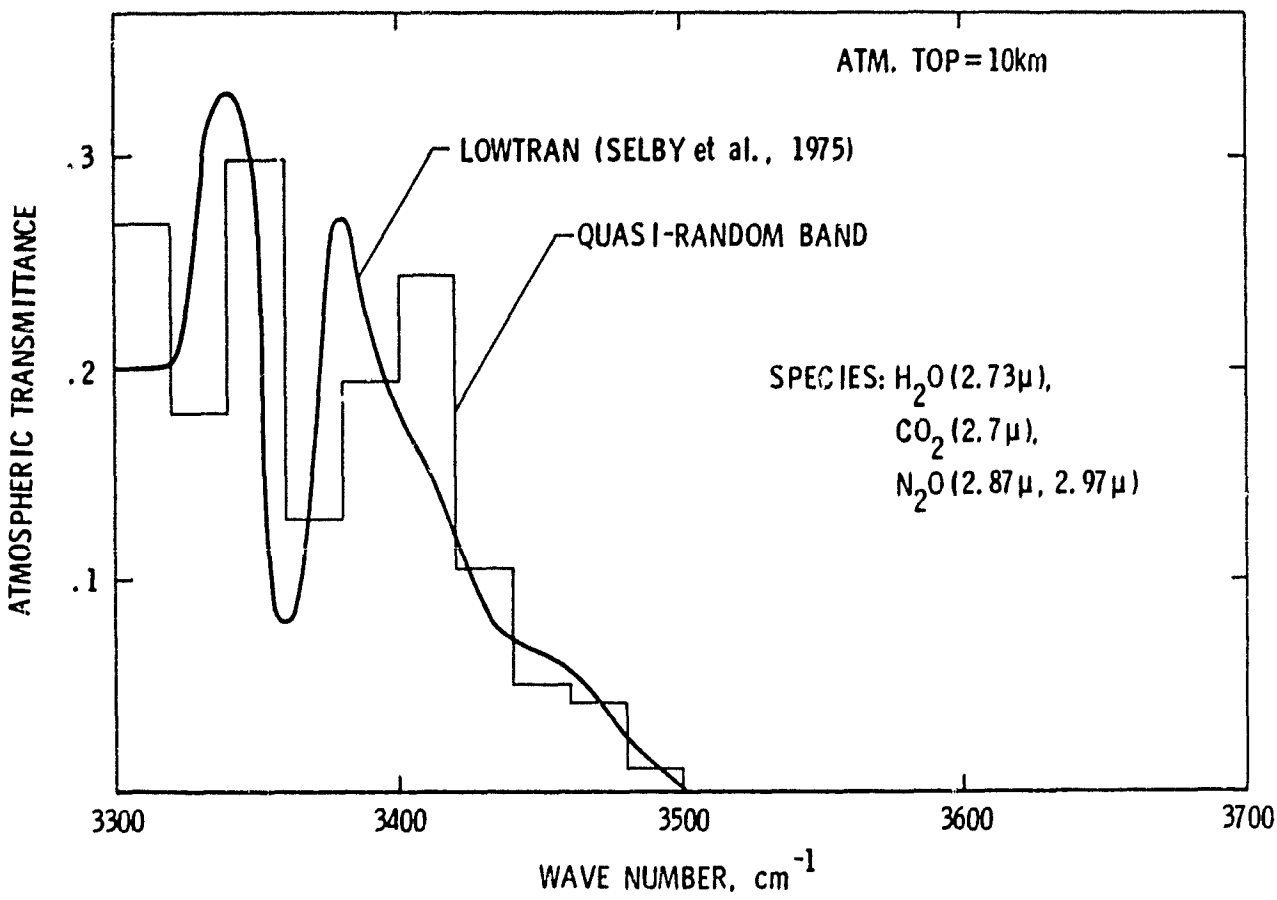

Figure 17. Comparison of atmospheric transmittance in the spectral range from 3300 to 3700 cm^{-1}.

The transmittance results for the spectral range from 2500 to 2800 cm^{-1} are shown in figures 18 and 19. The transmittance results as calculated by the QRB and LBL models and the LOWTRAN program by considering only the 3.17-μ water vapor band are shown in figure 18. The results are seen to be in good agreement. The results presented in figure 19 are also for the same spectral range as for figure 18, but in this case contributions of other bands (3.57-μ O_3, 3.85-μ CH_4, and 4.5-μ N_2O) have been included in calculating the atmospheric transmittance. From a comparison of results presented in these figures it may be concluded that the QRB results are in good agreement with the LBL and LOWTRAN results and that the transmittance (in this spectral range) is mainly due to the 3.17-μ H_2O band.

The results for the spectral range from 1800 to 2000 cm^{-1} are shown in figure 20. The contributions of all the important bands in this spectral range (6.27-μ H_2O, 5.2-μ CO_2, and 4.5-μ N_2O) were considered in calculation of the transmittance. The QRB results are seen to be in good agreement with the LOWTRAN results.

The results presented in figure 21 are for the spectral range from 500 to 800 cm^{-1}. The contributions of all the important molecular bands (20-μ H_2O, 15-μ CO_2, 14.3-μ O_3, and 17-μ N_2O) were considered in calculation of the transmittance. The QRB results are seen to be in general agreement with the LOWTRAN results.

Upwelling Atmospheric Radiance

For the standard atmospheric conditions, the results for upwelling radiance have been obtained for two different spectral ranges (2500-2800 cm^{-1} and 3300-3700 cm^{-1}) by employing the QRB model. The top of the atmosphere was again taken to be at 10 km. The contribution of the reflected component of solar radiation was included in calculation of the upwelling radiance, but the contribution of atmospheric radiation reflected from the surface was neglected.

In figure 22, the results are presented for the spectral range from 2500 to 2800 cm^{-1}. The molecular species whose contributions are included in this range are H_2O (3.17 μ), O_3 (3.57 μ) CH_4 (3.85 μ) and N_2O (4.5 μ).

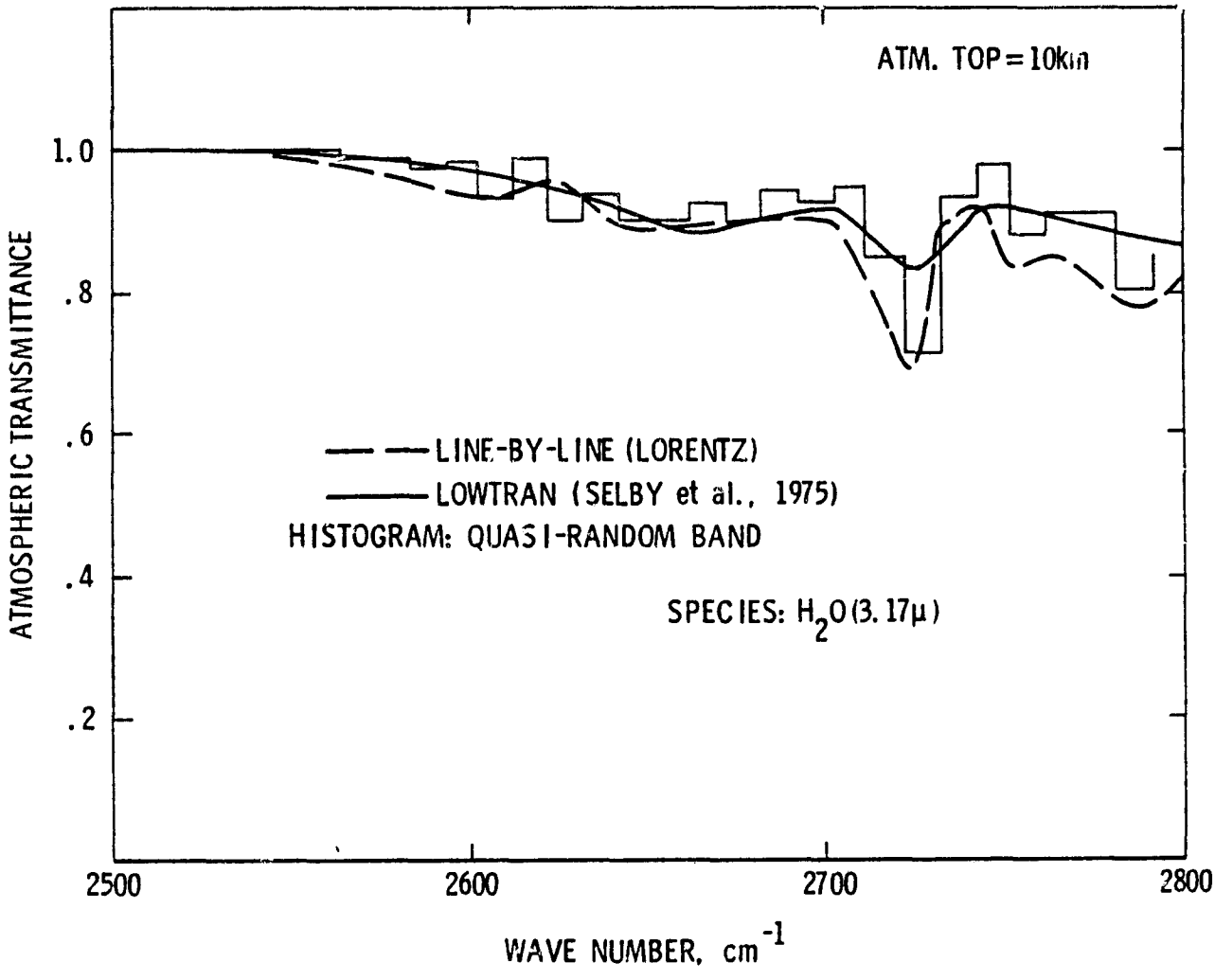

Figure 18. Comparison of atmospheric transmittance in the spectral range from 2500 to 2800 cm^{-1} considering water vapor only.

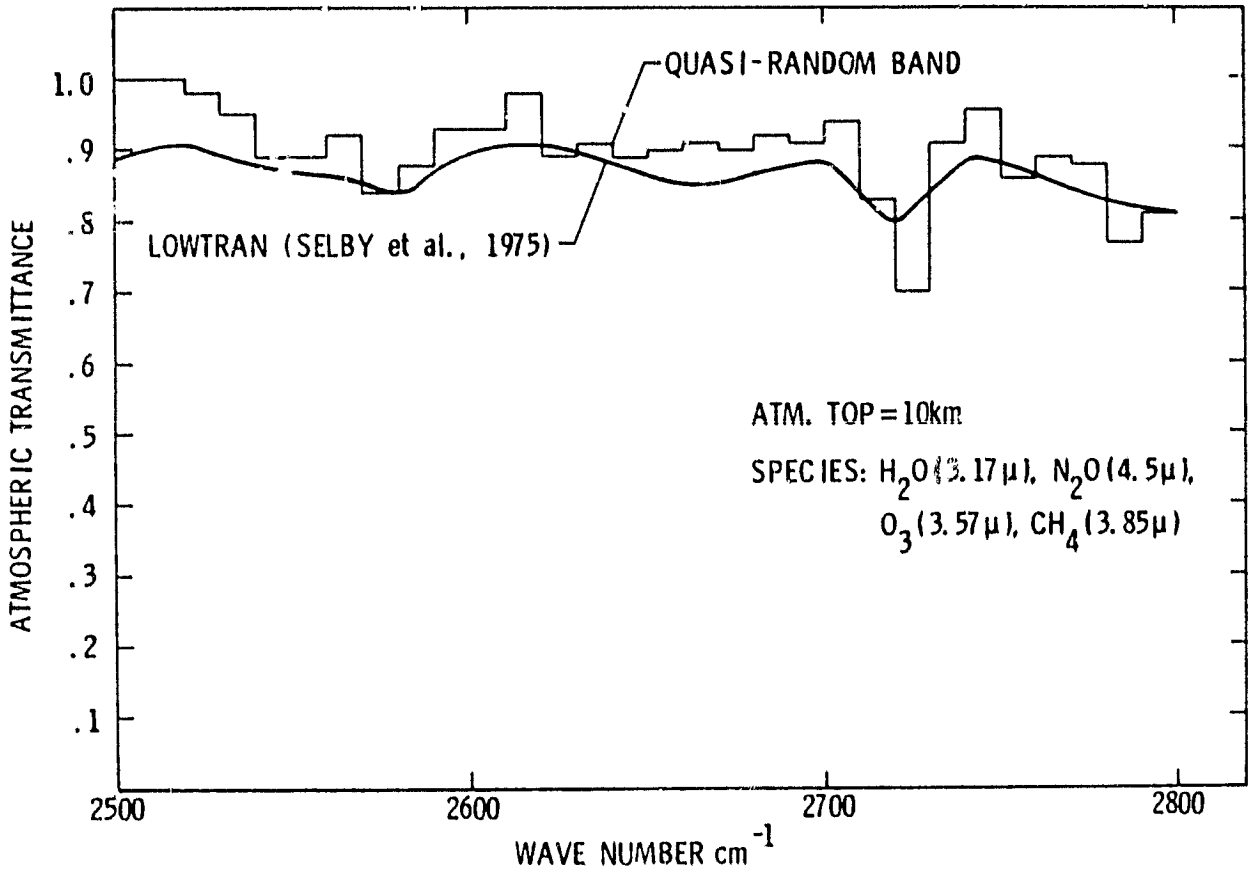

Figure 19. Comparison of atmospheric transmittance in the spectral range from 2500 to 2800 cm^{-1}.

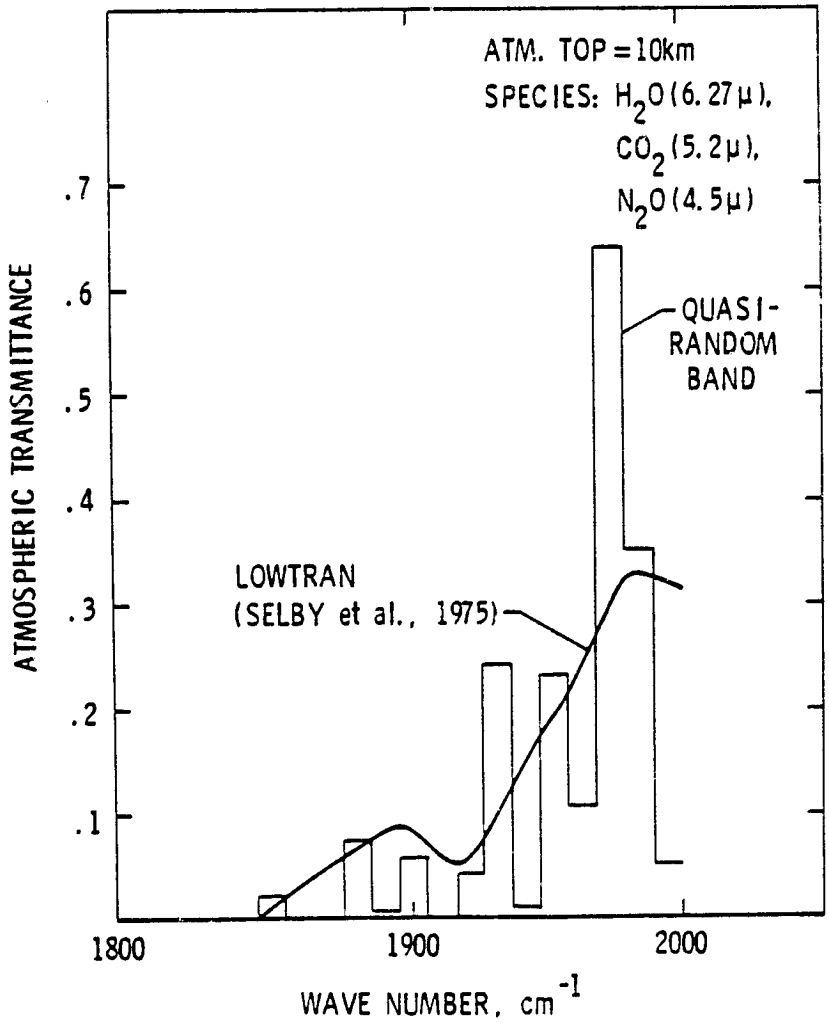

Figure 20. Comparison of atmospheric transmittance in the spectral range from 1800 to 2000 cm^{-1}.

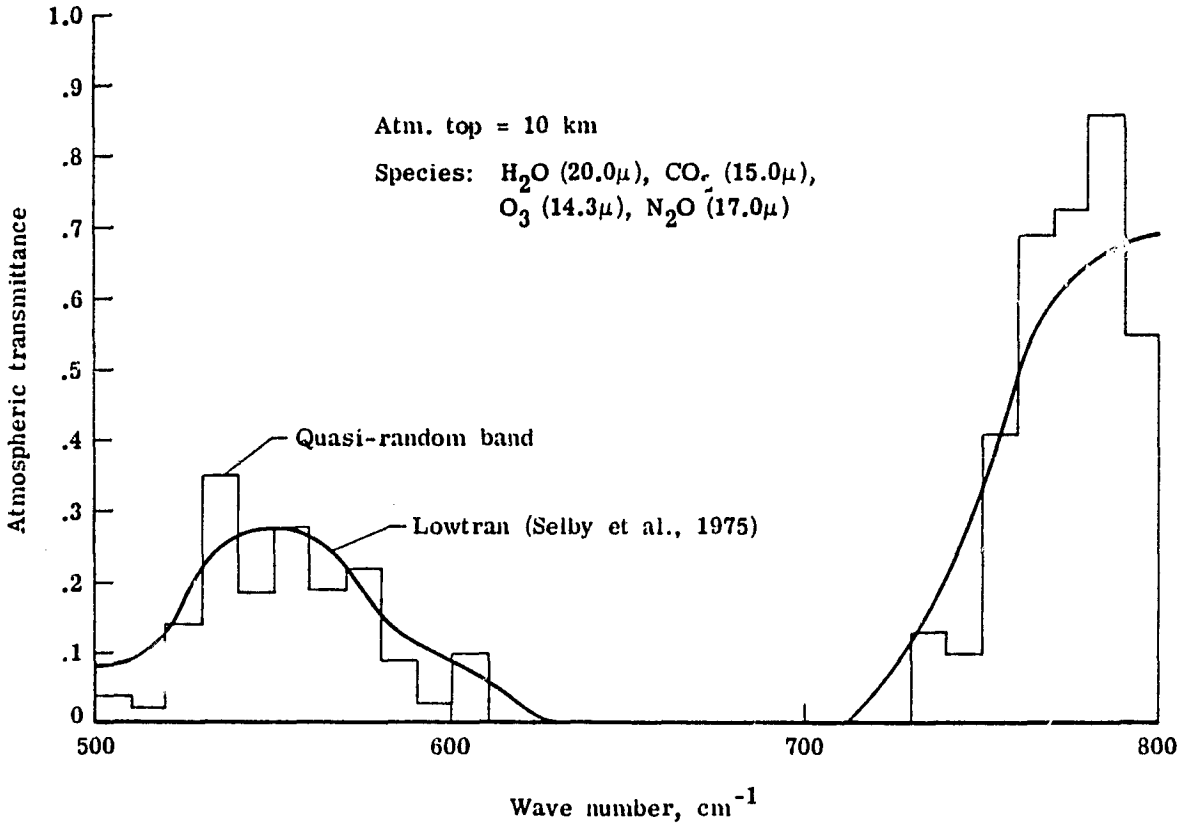

Figure 21. Comparison of atmospheric transmittance in the spectral range from 500 to 800 cm^{-1}.

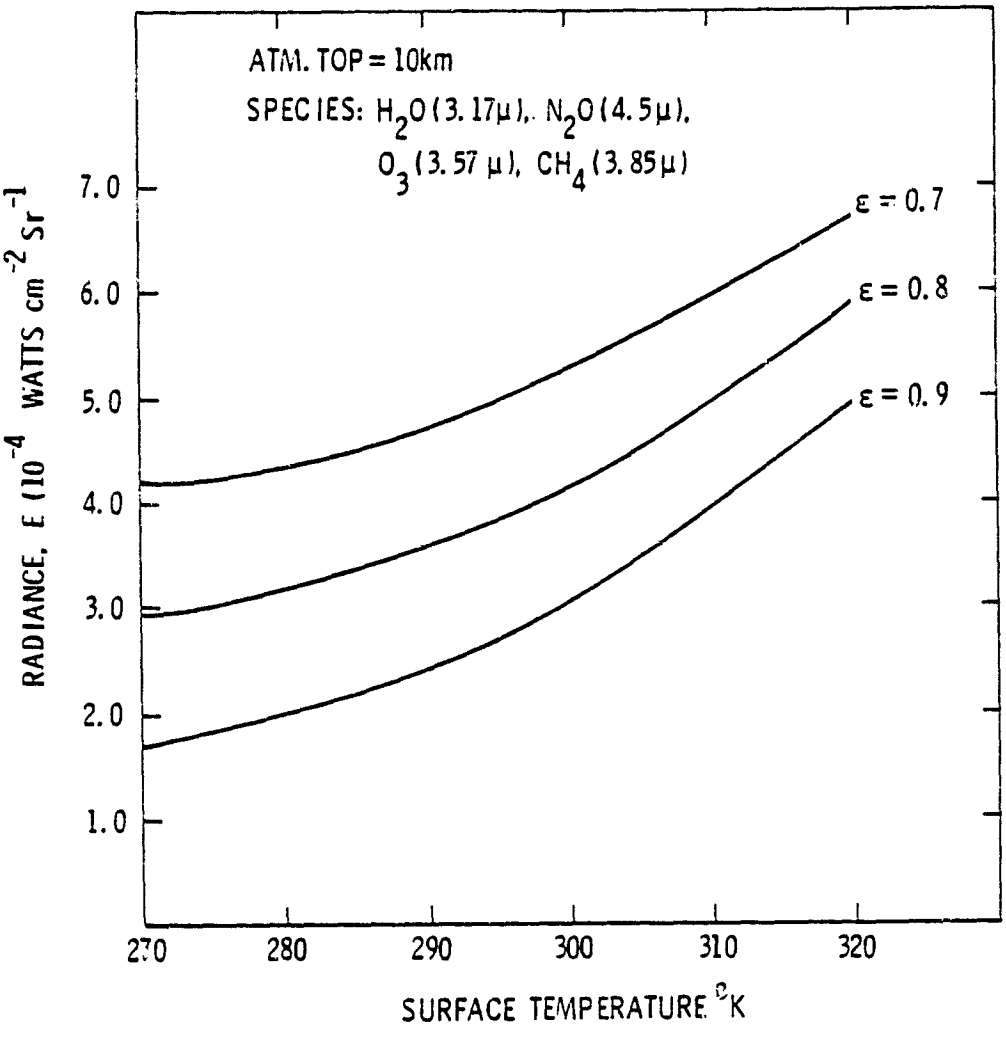

Figure 22. Upwelling radiance as a function of surface temperature (spectral range from 2500 to 2800 cm^{-1}).

The figure shows the variation of upwelling radiance with the surface temperature for different values of the surface emittance. For a fixed surface emittance, the upwelling radiance is seen to increase with increasing surface temperature. This is because the surface and atmospheric emissions are relatively higher at higher surface temperatures. For a fixed surface temperature, the upwelling radiance is seen to increase with decreasing surface emittance. This is because, for lower surface emittance, the reflected component of the solar radiation is larger, and this makes the total upwelling radiance relatively higher.

The results of upwelling radiance as a function of surface emittance are illustrated in figure 23 for different surface temperatures. These results were obtained for the spectral range from 3300 to 3700 cm^{-1} with contributions of 2.7-μ CO_2, 2.73-μ H_2O, 2.87-μ N_2O, and 2.97-μ N_2O bands included. The results show the same general trend as seen in figure 22. For a fixed surface temperature, it is possible for the upwelling radiance to increase with increasing surface emittance if the reflected component of solar radiation is not included.

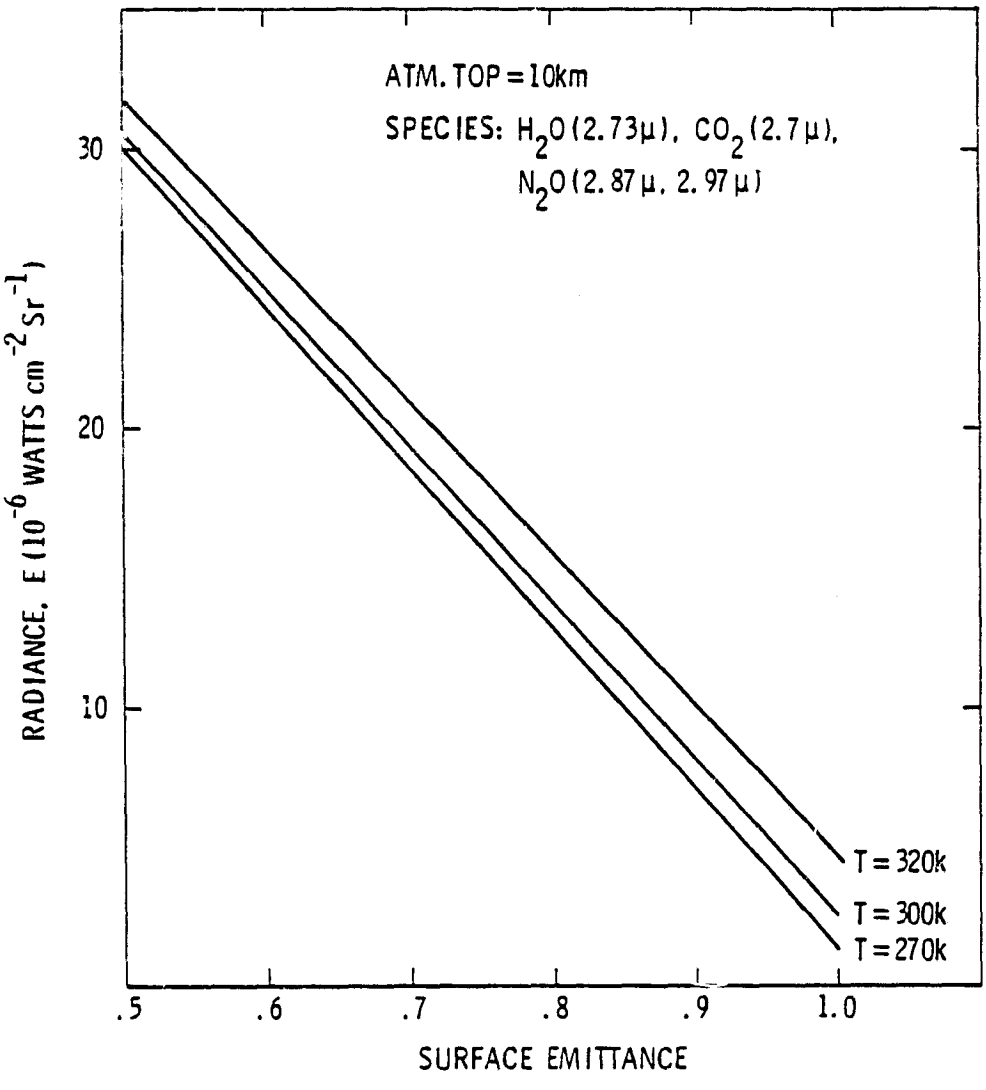

Figure 23. Upwelling radiance as a function of surface emittance (spectral range from 3300 to 3700 cm^{-1}).

CONCLUSIONS

Spectral and atmospheric transmittances have been calculated by different procedures to validate the quasi-random band model. The spectral transmittance and total band absorptance were evaluated for selected molecular bands (7.66-μ CH_4, 4.5-μ N_2O, 2.73-μ H_2O, 1.87-μ H_2O, and 2.7-μ CO_2) by using the LBL and QRB models and compared with the experimental results. The total band absorptance was evaluated also by using the ESFT and empirical correlations for H_2O and CO_2 bands, respectively. Atmospheric transmittances were calculated by the LBL and QRB models and compared with the results of the LOWTRAN program. Upwelling atmospheric radiances were calculated in two different spectral ranges to demonstrate the application of the QRB model.

For homogeneous conditions, comparison of transmittance and total band absorptance results obtained by different spectral models indicate that, for all bands, the QRB results are in good agreement with the LBL model and experimental results for most pressures and path lengths. The LBL model provides the best procedure for evaluating the transmittance, but is not practical because of high computational costs. The ESFT method has been found applicable only in a few cases. The results obtained by using the empirical correlations are not in good agreement with other results. Hence, use of the ESFT relation and other empirical correlations cannot be justified for atmospheric studies.

Comparison of atmospheric transmittance, as calculated by the QRB model and LOWTRAN program, indicates that the QRB results are in good agreement with the LOWTRAN results for all spectral ranges considered. In the spectral range from 2,500 to 2,800 cm^{-1}, results obtained by considering the contribution of only the 3.17-μ H_2O band indicate that the QRB results compare well with LBL and LOWTRAN results. From these comparisons, it may be concluded that the QRB model is computationally fast and accurate and, therefore, quite suitable for most atmospheric applications. The procedure for calculating the upwelling atmospheric radiance has been developed by using the QRB model. For the standard atmospheric conditions, the results for upwelling radiance have been obtained to demonstrate the use of the QRB model. The procedure can be used for extensive parametric

studies (surface as well as atmospheric) of atmospheric radiance. The program can be adapted easily for the Earth radiation budget and climate modeling studies.

APPENDIX A

QUASI-RANDOM COMPUTER PROGRAM TO CALCULATE ATMOSPHERIC TRANSMITTANCE AND UPWELLING RADIANCE

Computer Program QSRBAND

```
 PROGRAM QSRBAND(INPUT,OUTPUT,TAPE7,TAPE8,TAPE9,TAPE10)
 INTEGER X,G,W
 DIMENSION WN(5),HS(5),GR(5),HL(50),PCK(6,50,11),RADNC(6,50)
 DIMENSION FR1(2000),SA1(2000),AL1(2000),EL1(2000),
/FR2(370),SA2(370),AL2(370),EL2(370),FR3(1600),
/SA3(1600),AL3(1600),EL3(1600),FR4(820),SA4(820),AL4(820),EL4(820)
 DIMENSION TRH(50,11),TRC(50,11),TRN(50,11),TRHO(50),TRCO(50),
/TRNO(50),VPF(10,4),TRO(50,11),TROZ(50),RADNCE(6),TEMS(6)
 DIMENSION QN(10,4),TRA(50,11),TRM(11),TRT(50)
 COMMON X1(26),T1(26),X2(21),T2(21),FRB(50),FRC(50),TRG(50,11),
/PREC(10),TEMC(10),QQ(10),DEL,PNTP,TNTP,TEMR,KR,LC,JD,VP(10)
 READ 12,FRL,FRU,DEL,PNTP,TNTP,TEMR,RP1,RP2,RP3,RP4
 PRINT12,FRL,FRU,DEL,PNTP,TNTP,TEMR,RP1,RP2,RP3,RP4
 READ 11,LC,NG,LE1,LE2,LE3,JD,LE4
 PRINT11,LC,NG,LE1,LE2,LE3,JD,LE4
 READ 11,NG1,NG2,NG3,NG4
 PRINT11,NG1,NG2,NG3,NG4
 READ 16,(PREC(L),L=1,LC)
 PRINT16,(PREC(L),L=1,LC)
 READ 12,(TEMC(L),L=1,LC)
 PRINT12,(TEMC(L),L=1,LC)
 READ 10,((QN(L,G),L=1,LC),G=1,NG)
 PRINT10,((QN(L,G),L=1,LC),G=1,NG)
 READ 10,((VPF(L,G),L=1,LC),G=1,NG)
 PRINT10,((VPF(L,G),L=1,LC),G=1,NG)
 READ 15,(X1(W),W=1,26)
 PRINT15,(X1(W),W=1,26)
 READ 15,(T1(W),W=1,26)
 PRINT15,(T1(W),W=1,26)
 READ 15,(X2(W),W=1,21)
 PRINT15,(X2(W),W=1,21)
 READ 15,(T2(W),W=1,21)
 PRINT15,(T2(W),W=1,21)
 READ 12,EMI,ZEN
 PRINT12,EMI,ZEN
 READ 12,(WN(N),N=1,5)
```

```
      PRINT12,(WN(N),N=1,5)
      READ 16,(HS(N),N=1,5)
      PRINT16,(HS(N),N=1,5)
      READ 12,(TEMS(KK),KK=1,6)
      PRINT12,(TEMS(KK),KK=1,6)
      READ(7,20) (FR1(X),SA1(X),AL1(X),EL1(X),X=1,LE1)
      READ(8,20) (FR2(X),SA2(X),AL2(X),EL2(X),X=1,LE2)
      READ(9,20) (FR3(X),SA3(X),AL3(X),EL3(X),X=1,LE3)
      READ(10,20) (FR4(X),SA4(X),AL4(X),EL4(X),X=1,LE4)
   10 FORMAT(8F10.4)
   11 FORMAT(16I5)
   12 FORMAT(10F8.2)
   15 FORMAT(10F8.4)
   16 FORMAT(8E10.4)
   20 FORMAT(2(F10.3,E10.3,F5.3,F10.3,5X))
      RK=(FRU-FRL)/DEL+0.1
      KR=RK
      DELA=0.5*DEL
      FRB(1)=FRL
      DO 100 K=1,KR
      FRB(K+1)=FRB(K)+DEL
  100 FRC(K)=FRB(K)+DELA
      LB=LC+1
      DO 101 L=1,LB
      DO 101 K=1,KR
  101 TRA(K,L)=1.
      IF(NG1-1)102,103,102
  103 CONTINUE
      DO 104 L=1,LC
      VP(L)=VPF(L,1)
  104 QG(L)=QN(L,1)
      CALL ASHOK(FR1,SA1,EL1,LE1,AL1,RP1)
      DO 105 L=1,LB
      DO 105 K=1,KR
      TRH(K,L)=TRG(K,L)
  105 TRA(K,L)=TRA(K,L)*TRG(K,L)
  102 IF(NG2-2)106,107,106
  107 CONTINUE
      DO 108 L=1,LC
      VP(L)=VPF(L,2)
  108 QG(L)=QN(L,2)
      CALL ASHOK(FR2,SA2,EL2,LE2,AL2,RP2)
      DO 109 L=1,LB
      DO 109 K=1,KR
      TRC(K,L)=TRG(K,L)
  109 TRA(K,L)=TRA(K,L)*TRG(K,L)
  106 IF(NG3-3)110,111,110
  111 CONTINUE
```

```
      DO 112 L=1,LC
      VP(L)=VPF(L,3)
  112 DG(L)=DN(L,3)
      CALL ASHOK(FR3,SA3,EL3,LE3,AL3,RP3)
      DO 113 L=1,LB
      DO 113 K=1,KR
      TRN(K,L)=TRG(K,L)
  113 TRA(K,L)=TRA(K,L)*TRG(K,L)
  110 IF(NG4-4)114,115,114
  115 CONTINUE
      DO 116 L=1,LC
      VP(L)=VPF(L,4)
  116 DG(L)=DN(L,4)
      CALL ASHOK(FR4,SA4,EL4,LE4,AL4,RP4)
      DO 117 L=1,LB
      DO 117 K=1,KR
      TRG(K,L)=TRG(K,L)
  117 TRA(K,L)=TRA(K,L)*TRG(K,L)
  114 CONTINUE
      DO144 L=1,LB
      TRM(L)=0.
      DO144 K=1,KR
  144 TRM(L)=TRM(L)+TRA(K,L)/KR
      DO 143 K=1,KR
      TRHO(K)=TRH(K,1)
      TRCO(K)=TRC(K,1)
      TRNO(K)=TRN(K,1)
      TRDZ(K)=TRD(K,1)
  143 TRT(K)=TRA(K,1)
      DO 401 N=1,4
  401 GR(N)=(HS(N+1)-HS(N))/(WN(N+1)-WN(N))
      DO 402 K=1,KR
      N=0
  403 N=N+1
      IF(FRC(K)-WN(N))402,404,404
  404 IF(FRC(K)-WN(N+1))405,403,403
  405 HL(K)=DEL*(HS(N)+GR(N)*(FRC(K)-WN(N)))
  402 CONTINUE
      CONS=18.*6.625*1.E-07
      CNST=6.625*0.3/1.38
      DO 406 KK=1,6
      DO 406 K=1,KR
      RNUM=DEL*CONS*FRC(K)**3
      EEX=CNST*FRC(K)
      PCK(KK,K,1)=RNUM/(EXP(EEX/TEMS(KK))-1.)
      DO 406 L=1,LC
      PCK(KK,K,L+1)=RNUM/(EXP(EEX/TEMC(L))-1.)
  406 CONTINUE
      ZEN=(ZEN/57.29578)
      GAM=1.+1./COS(ZEN)
```

```
      DO 407 KK=1,6
      RADNCE(KK)=0.
      DO 407 K=1,KR
      ROOM=(1.-EMI)*(COS(ZEN))*HL(K)*(TRT(K))**GAM
      RADNC(KK,K)=EMI*PCK(KK,K,1)*TRT(K)*1.E-07+ROOM
      DO 407 L=2,LB
      COMP=PCK(KK,K,L)*(TRA(K,L)-TRA(K,L-1))*1.E-07
      RADNC(KK,K)=RADNC(KK,K)+COMP
  407 RADNCE(KK)=RADNCE(KK)+RADNC(KK,K)
      PRINT 82
      DO 501 K=1,KR
  501 PRINT 83,FRB(K+1),TRHO(K),TRCO(K),TRNO(K),TROZ(K),TRT(K)
      DO 503 KK=1,6
  503 PRINT 85,TEMS(KK),RADNCE(KK)
   82 FORMAT(/,3X,'FREQ.      H2OTRANS.   CO2TRANS.    N2OTRANS.   O3TRANS.
     /     TOTAL TRANS.',/)
   83 FORMAT(2X,F10.5,4X,5F10.5)
   85 FORMAT(/,5X,F8.2,5X,E12.5)
      STOP
      END
```

Subroutine ASHOK for Program QSKBAND

```
      SUBROUTINE ASHOK(FR,SA,EL,LE,AL,RR,
      INTEGER X,W
      DIMENSION FR(2000),SA(2000),EL(2000),AL(2000),BIG(5),BI(2000),
     /BIG(6,50),LIB(50),LIE(50),MP(50),SBI(5,50),NBI(5,50),
     /BL(2000),AVBI(5,50),SUMBI(5,50)
      COMMON /1(26),T1(26),X2(21),T2(21),FRB(50),FRC(50),TRO(50),L,
     /FREQ(10),TEMC(10),QQ(10),DEL,FNTP,TNTP,TEMR,RR,LC,LB,VP(10)
      X=0
      DO 121 K=1,KR
      M=0
124   IF(X.GE.LE)GOTO123
      X=X+1
      IF(FR(X).LT.FRB(K))GOTO124
      IF(FR(X).GE.FRB(K+1))GOTO127
      M=M+1
      GOTO124
127   IF(K.GE.KR)GOTO123
      X=X-1
123   MP(K)=M
121   CONTINUE
      DO 151 K=1,KR
      DO 151 I=1,5
151   SUMBI(I,K)=0.
      LB=LC+1
      PI=3.1415926E4
      DELA=0.5*DEL
      ULB=0.
      BSU=0.
      DO 150 MM=1,LC
      L=LC+1-MM
      CST=(SQRT(TEMR/TEMC(L)))*FREQ(L)/FNTP
      PART=VP(L)*((TEMR/TEMC(L))**RR)*2.6*E+19
      FACT=1.439*(TEMC(L)-TEMR)/(TEMC(L)*TEMR)
      CONST=0.1*TNTP/FNTP
      PL=CONST*FREQ(L)*QQ(L)/TEMC(L)
      ALA=0.
      DO 201 X=1,LE
      BL(X)=CST*AL(X)
      ALA=ALA+BL(X)
201   BI(X)=SA(X)*PART*EXP(EL(X)*FACT)
      ALA=ALA/LE
      ULA =PL/(PI*ALA)
      BSU=BSU+ULA*ALA
      ULB =ULB+ULA
      ALB =BSU/ULB
      RHO =ALB/DELA
      X=0
      DO 206 K=1,KR
      IF(MP(K).EQ.0)GOTO206
      LIB(K)=X+1
```

```
      LIE(K)=LIB(K)+MP(K)-1
      X=LIE(K)
  206 CONTINUE
      DO 207 K=1,KR
      IF(MP(K).EQ.0) GO TO 219
      JB=LIB(K)
      JE=LIE(K)
      BIGI(K)=SI(JB)
      JC=JB+1
      DO 208 J=JC,JE
      IF(BIGI(K).GE.SI(J)) GO TO 208
      BIGI(K)=SI(J)
  208 CONTINUE
      DO 209 I=1,6
      IX=-I+1
  209 BIG(I,K)=BIGI(K)*10.**IX
      DO 210 I=1,5
      N=0
      SSI(I,K)=0
      DO 211 J=JB,JE
      IF(SI(J).GT.BIG(I,K)) GO TO 211
      IF(SI(J).LE.BIG(I+1,K)) GO TO 211
      N=N+1
      SSI(I,K)=SSI(I,K)+SI(J)
      NSI(I,K)=N
  211 CONTINUE
      IF(NSI(I,K).GE.1) GO TO 210
      NSI(I,K)=1
  210 AVSI(I,K)=SSI(I,K)/NSI(I,K)
      GO TO 207
  219 DO 220 I=1,5
      NSI(I,K)=1
  220 AVSI(I,K)=0
  207 CONTINUE
      DO 310 K=1,KR
      DO 310 I=1,5
  310 SUMSI(I,K)=SUMSI(I,K)+AVSI(I,K)*ULA
      DO 212 K=1,KR
      TRG(K,L)=1.
      DO 213 J=1,KR
      TRD=1.
      JA=IABS(J-K)
      IF (JA.GT.JD) GO TO 213
      ZI=FRC(K)-FRC(J)
      EPSI=ZI/DELA
      DO 215 I=1,5
      NSJ=NSI(I,J)
      XI=SUMSI(I,J)
      RES=0.
      IF (J.NE.K) GO TO 216
      DO 217 W=1,26
      Z=RHO*RHO*XI/(X1(W)*X1(W)+RHO*RHO)
      IF (Z.GT.675.) GO TO 200
```

```
      Y=EXP(-Z)
      GO TO 217
  200 Y=0
  217 RES=RES+Y*T1(W)
      GO TO 215
  216 DO 218 W=1,21
      Z1=RHO*RHO*XI/((EPSI-X2(W))*(EPSI-X2(W)))
      IF (Z1.GT.675.) GO TO 300
      Y=EXP(-Z1)
      GO TO 218
  300 Y=0.
  218 RES=RES+Y*T2(W)
      RES=RES/6.
  215 TRD=TRD*(RES**NSJ)
  213 TRG(K,L)=TRG(K,L)*TRD
  212 CONTINUE
  150 CONTINUE
      DO 320 K=1,KR
  320 TRG(K,LB)=1.
      RETURN
      END
```

APPENDIX B

EXPLANATION OF SYMBOLS USED IN COMPUTER PROGRAM

Symbols Used in Program QSRBAND

AL1, AL2, AL3, AL4	average line width for the different molecules H_2O, CH_4, N_2O, and O_3, respectively.
DEL	width of an interval, cm^{-1}
EL1, EL2, EL3, EL4	energies of the lower states for the lines of the molecules, cm^{-1}
EM1	surface emittance
FRB	wave number at the interval boundaries, cm^{-1}
FRC	wave number at the interval centers, cm^{-1}
FRL	lower frequency limit of the range
FRU	upper frequency limit of the range
FR1, FR2, FR3, FR4	wave numbers of the lines of the molecules, cm^{-1}
GAM	$1 + f(\theta)$ where $f(\theta) = \sec \theta$ for $\theta \leq 60$ and $f(\theta) = Ch(\theta)$ for $\theta > 60$; $Ch(\theta)$ is the Chapman function
GR	gradients used in calculations of HL
HL	computed solar irradiance at the top of the atmosphere in an interval, W cm^{-2} sr^{-1}
HS	tabulated values of the solar irradiance at the top of the atmosphere, W cm^{-2} sr^{-1}
JD	number of adjacent intervals on both sides of an interval from which the contribution is taken into account
KR	number of intervals in the band
LC	number of layers into which atmosphere is divided (10)
LE1, LE2, LE3, LE4	total number of lines in the spectrum
NG	total number of gases

NG1, NG2 NG3, NG4	identifying integers for the gases
PCK	Planck's function
PNTP	pressure at NTP, bar
PREC	pressure at the different layers, bar
QN	altitude distribution of the molecules H_2O, CH_4, N_2O, and O_3, respectively
RADNC	radiance in each interval
RADNCE	integrated radiance
RCOM	radiance component due to reflected solar radiation
RP1, RP2 RP3, RP4	exponent to account for the temperature dependence of the rotational partition function for the molecules
SA1, SA2 SA3, SA4	intensity of the individual lines
TEMC	temperature at the center of the layers, K
TEMR	reference temperature for the line parameters, K
TEMS	surface temperature, K
TNTP	temperature at NTP, K
TRA	combined transmittance of all the interferring gases
TRCO	transmittance due to CH_4 only between the top of the atmosphere and surface
TRHO	transmittance due to H_2O only between the top of the atmosphere and surface
TRNO	transmittance due to N_2O only between the top of the atmosphere and surface
TROZ	transmittance due to O_3 only between the top of the atmosphere and surface
TRT	combined transmittances of all the interfering gases for each interval between the top of the atmosphere and surface
X_1, T_1	convolution parameters for integration of direct contribution
X_2, T_2	convolution parameters for the integration of wing contribution

VPF	vibrational partition functions for H_2O, CH_4, N_2O, and O_3
WN	wave numbers at which the solar irradiance at the top of the atmosphere is considered

Symbols Used in Subroutine ASHOK

ALA	altitude-dependent average width of the lines of a molecule
ALB	altitude-dependent individual width of the lines of a molecule
AVSI	average value of intensity for the lines in one decade in an interval
BIG	intensity values separating the five decades in each interval
BIGI	intensity of the strongest line in an interval
FACT	factor used in the computation of altitude dependence of integrated intensity
JB	number of adjacent intervals from which the wing contribution is considered
LIB	serial number of the first line in an interval
LIE	serial number of the last line in an interval
MP	number of lines in an interval
NSI	number of lines in a decade within an interval
SSI	sum of the intensities of all the lines within one decade of an interval
SUMSI	optical thickness between the top of the atmosphere and the altitude under consideration

REFERENCES

1. Wark, D.Q., Yamamoto, G.; and Lienesch, J.H.: Methods of Estimating Infrared Flux and Surface Temperature from Meteorological Satellites. J. Atmos. Sci., Vol. 19, Sept. 1962, pp. 369-384.

2. Lenschow, D.H.; and Dutton, J.A.: Surface Temperature Variations from an Airplane over Several Surface Types. J. Appl. Meteor., Vol. 3, Feb. 1964, pp. 65-69.

3. Marlatt, W.E.; Harlan, J.C.; and Cole, H.L.: Mathematical Models for Radiation Transfer. Dept. of Watershed Sciences, Colorado State Univ. (Fort Collins, Colo.), 1971.

4. Tiwari, S.N.: Models for Infrared Atmospheric Radiation. Final Report, NASA grant NSG 1153, June 1976. Also in Advances in Geophysics, Vol. 20, Academic Press, 1978, pp. 1-85.

5. Cess, R.D.: Radiative Transfer Due to Atmospheric Water Vapor: Global Considerations of the Earth's Energy Balance. J. Quant. Spectrosc. Radiat. Transfer, Vol. 14, No. 9, Sept. 1974, pp. 861-872.

6. Ramanathan, V.: Radiative Transfer within the Earth's Troposphere and Stratosphere. A Simplified Radiative-Convective Model. J. Atmos. Sci., Vol. 33, No. 7, July 1976, pp. 1330-1346.

7. Arking, A.; Chesters, D.; and Chow, M.D.: Fast but Accurate Techniques for Calculating Radiative Terms in Numerical Atmospheric Models and in Remote Sensing Applications. Paper No. 35, Third NASA Weather and Climate Program Science Review, Conference Publication 2029, 1977, pp. 195-200.

8. Smith, W.L.; Hickey, J.; Howell, H.B.; Jacobwitz, H.; Hilleary, D.T.; and Drummond, A.J.: Nimbus-6 Earth Radiation Budget Experiment. Appl. Opt., Vol. 16, No. 2, Feb. 1977, pp. 306-318.

9. Woerner, C.V.; and Cooper, J.E.: Earth Radiation Budget Satellite System Studies. NASA TM X-72776, 1977.

10. Wyatt, P.J.; Stull, V.R.; and Plass, G.N.: Quasi-Random Model of Band Absorption. J. Opt. Soc. Amer., Vol. 52, No. 11, Nov. 1962, pp. 1209-1217.

11. Kunde, V.G.: Theoretical Computations of the Outgoing Infrared Radiance from a Planetary Atmosphere. NASA TN D-4045, Aug. 1967.

12. Gupta, S.K.; and Tiwari, S.N.: Evaluation of Upwelling Infrared Radiance from Earth's Atmosphere. Progress Report, NASA grant NSG 1153, Nov. 1975.

13. Wiscombe, W.J.; and Evans, J.N.: Exponential-Sum Fitting of Radiative Transmission Functions. J. Comput. Phys., Vol. 24, No. 4, Aug. 1977, pp. 416-444.

14. Sasamori, T.: The Radiative Cooling Calculation for Application to General Circulation Experiments. J. Appl. Meteor., Vol. 7, No. 5, Oct. 1968, pp. 721-729.

15. Sasamori, T.: Simplification of Radiative Cooling Calculation for Application to Atmospheric Dynamics. WMO Tech. Note 104, 1970, pp. 479-488.

16. Rasool, S.I.; and Schneider, S.H.: Atmospheric Carbon Dioxide and Aerosols: Effects of Large Increases on Global Climate. Science, Vol. 173, 1971, pp. 138-141.

17. Rodgers, C.D.: Modeling of Atmospheric Radiation for Climatic Studies. The Physical Basis of Climate and Climate Modeling, GARP Publication Series, No. 16, pp. 177-180.

18. Fels, S.B.; and Kaplan, L.D.: A Test of the Role of Longwave Radiative Transfer in a General Circulation Model. J. Atmos. Sci., Vol. 32, No. 4, April 1975, pp. 779-789.

19. Kunde, V.G.; and Maguire, W.C.: Direct Integration Transmittance Model. J. Quant. Spectrosc. Radiat. Transfer, Vol. 14, No. 8, Aug. 1974, pp. 806-814.

20. Tiwari, S.N.; and Gupta, S.K.: Accurate Spectral Modeling for Infrared Radiation. J. Heat Transfer, Vol. 100, May 1978, pp. 240-246.

21. Burch, E.E.; Gryvnak, D.A.; Singleton, E.B.; France, W.L.; and Williams, D.: Infrared Absorption by Carbon Dioxide, Water Vapor, and Minor Atmospheric Constituents. AFCRL-62-698, Air Force Cambridge Research Laboratories (Bedford, Mass.), July 1962.

22. Selby, J.E.A.; and McClatchey, R.A.: Atmospheric Transmittance from 0.25 to 28.5 m: Computer Code LOWTRAN 3. AFCRL-TR-75-0255, Air Force Cambridge Research Laboratories (Bedford, Mass.), 1975.

23. Sparrow, E.M.; and Cess, R.D.: Radiation Heat Transfer (Augmented Edition). Hemisphere Publishing Company, McGraw Hill Series in Thermal and Fluid Engineering, 1978.

24. Ludwig, C.B.; Griggs, M.; Malkmus, W.; and Bartle, E.R.: Air Pollution Measurements from Satellites. NASA CR-2524, Nov. 1973.

25. Ramanathan, V.: Satellite Radiation Budget Measurements in Spectral Bands. Earth Radiation Budget Science 1978, NASA Conference Publication 2100 (NASA CP-2100), Oct. 1979, pp. 66-68.

26. Mitchell, A.C.G.; and Zemansky, W.M.: Resonance Radiation and Excited Atoms. Harvard Univ. Press (Cambridge, Mass.), 1934.

27. Plass, G.N.: Models for Spectral Band Absorption. J. Opt. Soc., Vol. 48, Oct. 1958, pp. 690-703.

28. Penner, S.S.: Quantitative Molecular Spectroscopy and Gas Emissivities. Addison-Wesley (Reading, Mass.), 1959.

29. Goody, R.M.: Atmospheric Radiation I: Theoretical Basis. Oxford Univ. Press (London and New York), 1964.

30. Kondratyev, K.Y.: Radiation in Atmosphere. Academic Press (N.Y.), 1969.

31. Armstrong, B.H.; and Nicholls, R.W.: Emission, Absorption and Transfer of Radiation in Heated Atmosphere. Pergamon Press (Oxford), 1972.

32. Howard, J.N.; Burch, D.E., and Williams, D.: Infrared Transmissions Through Synthetic Atmospheres III, Absorption by Water. J. Opt. Soc. Amer., Vol. 46, Apr. 1956, pp. 242-245.

33. Liou, Kuo-Nan; and Sasamori, T.: On the Transfer of Solar-Radiation in Aerosol Atmospheres. J. Atmos. Sci., Vol. 32, Nov. 1975, pp. 2166-2177.

34. Stephens, G.L.: Radiation Profiles in Extended Water Clouds I: Theory. J. Atmos. Sci., Vol. 35, Nov. 1978, pp. 2111-2122.

35. Howard, J.N.; Burch, D.E.; Williams, D.: Infrared Transmission of Synthetic Atmosphere II, Absorption by Carbon Dioxide. J. Opt. Soc. Amer , Vol. 46, Apr. 1956, pp. 237-241.

36. McClatchey, R.A.; Fenn, R.W.; Selby, J.E.A.; Volz, F.E.; and Garing, J.S.: Optical Properties of the Atmosphere (3rd ed.). AFCRL-72-0497, Air Force Cambridge Research Laboratories (Bedford, Mass.), 1972.

37. McClatchey, R.A.; Benedict, W.S.; Clough, S.A.; Burch, D.E.; Calfee, R.F.; Fox, K.; Rothman, L.S.; and Garing, J.S.: AFCRL Atmospheric Line Parameters Compilation. AFCRL-TR-73-0096, Air Force Cambridge Research Laboratories (Bedford, Mass.), Jan. 1973.

38. U.S. Standard Atmosphere, 1962, U.S. Govt. Printing Office (Washington, D.C.), 1962.